

---

# VL-SAE: Interpreting and Enhancing Vision-Language Alignment with a Unified Concept Set

---

Shufan Shen<sup>1,2</sup> Junshu Sun<sup>1,2</sup> Qingming Huang<sup>1,2</sup> Shuhui Wang<sup>1\*</sup>

<sup>1</sup>State Key Lab. of AI Safety, Institute of Computing Technology, Chinese Academy of Sciences

<sup>2</sup>University of Chinese Academy of Sciences

{shenshufan22z, sunjunshu21s, wangshuhui}@ict.ac.cn qmhuang@ucas.ac.cn

## Abstract

The alignment of vision-language representations endows current Vision-Language Models (VLMs) with strong multi-modal reasoning capabilities. However, the interpretability of the alignment component remains uninvestigated due to the difficulty in mapping the semantics of multi-modal representations into a unified concept set. To address this problem, we propose VL-SAE, a sparse autoencoder that encodes vision-language representations into its hidden activations. Each neuron in its hidden layer correlates to a concept represented by semantically similar images and texts, thereby interpreting these representations with a unified concept set. To establish the neuron-concept correlation, we encourage semantically similar representations to exhibit consistent neuron activations during self-supervised training. First, to measure the semantic similarity of multi-modal representations, we perform their alignment in an explicit form based on cosine similarity. Second, we construct the VL-SAE with a distance-based encoder and two modality-specific decoders to ensure the activation consistency of semantically similar representations. Experiments across multiple VLMs (*e.g.*, CLIP, LLaVA) demonstrate the superior capability of VL-SAE in interpreting and enhancing the vision-language alignment. For interpretation, the alignment between vision and language representations can be understood by comparing their semantics with concepts. For enhancement, the alignment can be strengthened by aligning vision-language representations at the concept level, contributing to performance improvements in downstream tasks, including zero-shot image classification and hallucination elimination. Codes are available at <https://github.com/ssfgunner/VL-SAE>.

## 1 Introduction

Vision-Language Models (VLMs) have demonstrated remarkable capabilities in multi-modal understanding and reasoning, largely attributed to the various training objectives [22, 41] and architectures [57, 27, 66, 65] that effectively align the semantics of vision and language representations. This alignment mechanism serves as a core component of VLMs, enabling them to make predictions by integrating information from both modalities [41, 34, 60, 27, 55, 17]. Nevertheless, current comprehension of the alignment mechanism remains insufficient [13, 49, 38, 2]. This limited comprehension hinders our ability to analyze and address the misalignment cases, such as hallucinations [33, 26, 21]. To tackle this challenge, existing methods interpret representations of VLMs by mapping their semantics to concepts. However, these methods either solely focus on the vision [32, 2] or the language [38] representations, as shown in Figure 1(a). It remains an open problem to interpret the vision-language alignment, which requires not only understanding the representation semantics but also comparing the semantics of both modalities in an interpretable manner [49].

---

\*Corresponding author.

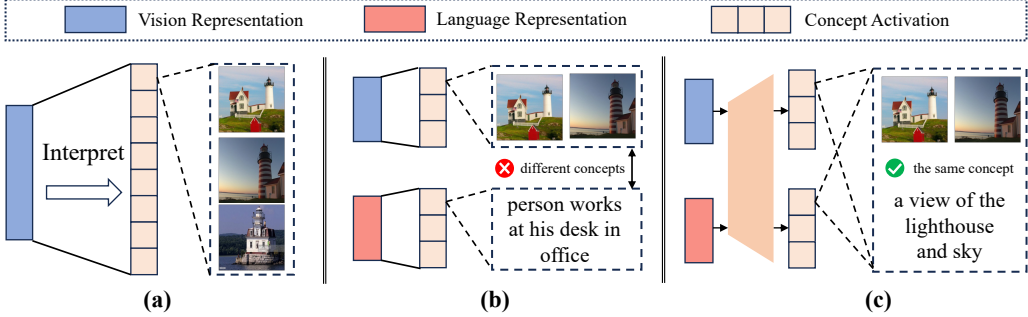


Figure 1: (a) Current interpretation methods are designed for single-modal representations. (b) Using current methods for each modality leads to a mismatch in the concept sets, hindering the interpretation of the vision-language alignment. (c) We propose the VL-SAE to interpret the alignment mechanism by mapping the representation semantics of both modalities into a unified concept set.

A straightforward approach to address this problem is to apply existing methods [46, 8] to map the representation semantics of each modality to concepts separately. With these concepts, we can compare the semantics of vision and language representations for interpreting their alignment mechanism. However, current methods struggle to conduct this comparison with concepts, *as they cannot effectively map the semantics of vision and language representations into a unified concept set*. These methods acquire the concept set in a pre-defined [24, 46, 2] or learnable [35, 8, 32] manner. Pre-defined methods rely on manually constructed concept sets, which often fail to capture the full spectrum of representation semantics [46, 63] and suffer from limited scalability due to the need to collect labeled samples for each concept [24]. Learnable methods employ the hidden activations of a pre-trained sparse autoencoder (SAE) to acquire the concept set, where each hidden neuron correlates to a concept and is defined by the samples that most strongly activate it. The neuron-concept correlation is established via end-to-end learning under self-supervision, eliminating the need for concept-specific annotations [8, 32]. Nevertheless, the end-to-end learning introduces uncontrollability into the concept set. Due to the uncontrollability, applying two separate SAEs to vision and language representations respectively causes the concept mismatch, *i.e.*, neurons at the same location of different SAEs being correlated with different concepts, as illustrated in Figure 1(b). As a result, semantically similar vision and language representations can exhibit inconsistent activations under concept mismatch, hindering the comparisons of representation semantics with SAE.

As the concept mismatch stems from applying separate SAEs to different modalities, using a shared SAE for both modalities seems to be a promising solution. By encouraging semantically similar representations to exhibit consistent activations during self-supervised training, the hidden layer neurons can be co-activated by semantically similar images and texts as shown in Figure 1(c), thereby mitigating the concept mismatch. Unfortunately, current SAEs designed for single-modal scenarios fail to achieve this objective for two primary reasons. (i) In contrast to single-modal representations that use the inner product for measuring semantic similarity, multi-modal representations of different VLMs exhibit varying alignment strategies [34, 27, 43], which complicates the measurement of their semantic similarity. (ii) Multi-modal representations exhibit modality-specific distributions [50], making it difficult to ensure the activation consistency of semantically similar representations.

In this paper, we propose the VL-SAE, an SAE architecture equipped with an auxiliary autoencoder, to mitigate the concept mismatch. We perform the representation alignment in an explicit form with the auxiliary autoencoder to measure their semantic similarity and then employ VL-SAE to constrain the activation consistency among semantically similar representations. Specifically, (i) for the alignment strategy, we propose an auxiliary autoencoder that maps the original representations to its intermediate representations. The autoencoder is optimized via contrastive loss [43] to ensure that vision-language representations with higher semantic similarity exhibit greater cosine similarity between their intermediate representations. (ii) For the architecture of VL-SAE, we propose an encoder that activates neurons based on the Euclidean distance between normalized representations and neuron weights. This metric satisfies the triangle inequality and is related to the cosine similarity, which correlates with semantic similarity rather than distributional information. These properties ensure that only semantically similar representations can be close to the same weights and activate corresponding neurons. Additionally, we propose separate decoders to capture the distributional information of each modality for representation reconstruction, thereby preventing the encoder from embedding modality-specific information into neuron activations that leads to concept mismatch.

In experiments, we construct VL-SAE on multiple VLMs, including Contrastive VLMs (CVLMs) [43] that achieve alignment via retrieval tasks and Large VLMs (LVLMs) [34, 1] that rely on question answering tasks. Evaluations of the proposed VL-SAE and current architectures [8, 15] demonstrate that VL-SAE possesses superior ability for mapping the semantics of vision and language representations into a unified concept set. Subsequently, we utilize VL-SAE to interpret and enhance the vision-language alignment mechanism of VLMs. For interpretation, we explain the model prediction by visualizing the activated concepts of vision and language representations during inference. For enhancement, we propose two strategies to improve the performance of CVLM in zero-shot image classification [25, 59, 18] and LVLM in hallucination elimination [30] by enhancing the vision-language alignment at the concept level. The contributions of our work are as follows:

- We propose the VL-SAE, a model to interpret the alignment mechanism of VLMs by mapping the semantics of vision-language representations into a unified concept set.
- We apply VL-SAE on multiple widely-used VLMs and demonstrate the superior quality of the concept set learned by VL-SAE in experiments.
- We show that VL-SAE can be employed to interpret the model prediction by visualizing the activated concepts, enhancing the performance of CVLMs on zero-shot image classification, and eliminating the hallucinations of LVLMs.

## 2 Related Work

**Vision-Language Models.** To handle the vision-language reasoning tasks, researchers have developed multiple VLMs [41, 34, 1, 43, 60, 55, 17] by effectively aligning their vision and language representations. According to the pre-training tasks, these models can be categorized into Contrastive VLMs (CVLMs) [11, 43] that utilize retrieval tasks and Large VLMs (LVLMs) [34, 1, 60, 55, 17] that incorporate Large Language Models (LLMs) [56] for pre-training with question answering tasks. For CVLMs, current models include a vision encoder and a text encoder, applied with contrastive training strategies that encourage semantically similar representations to achieve high inner product values [11]. For LVLMs, existing methods compose the model with a vision encoder, an LLM, and a light-weight connector that maps the output of the vision encoder to input tokens of the LLM. Vision-language representations are implicitly aligned through pre-training with question answering tasks [57, 1]. Despite the various architectures and pre-training paradigms of VLMs, our proposed VL-SAE can interpret and enhance the alignment mechanism of their vision-language representations.

**Representation Interpretation.** Revealing the semantics of representations stands as one of the primary challenges tackled by interpretable machine learning [40]. Previous methods [24, 62, 64, 46] pre-define a concept set and then collect corresponding samples to derive concept vectors in the representation space. The representations are projected onto these vectors for interpretation. These methods are costly due to the requirements for constructing concept sets and collecting relevant samples [24]. Moreover, these methods encounter challenges in modifying model behavior by adjusting corresponding interpretations, as it is difficult to map these interpretations back to the original representations [46]. Recently, Sparse Autoencoder (SAE) [8, 32, 15, 28] has been recognized as an effective method to interpret representations and modify model behaviors through self-supervised learning. Despite achieving advanced performance, current SAEs remain unsuitable for vision-language representations due to the inconsistency between the learned concept sets of both modalities. To address this problem, we propose the VL-SAE with a distance-based encoder and two modality-specific decoders to interpret vision-language representations with a unified concept set.

**Understanding the Internal Mechanism of VLMs.** There has been an increasing interest in investigating the internal mechanisms of VLMs through the lens of multi-modality [9]. Neuron-based methods [16, 44, 37] reveal the existence of multi-modal neurons that translate vision information to corresponding information in text modality. These neurons are located through important scores like gradient [44] and metrics leveraging architecture information [37]. Representation-based methods attempt to interpret the semantics of vision-language representations with concepts. For CVLMs, SpLiCE [2] and TEXTSPAN [14] disentangle the vision representations of CLIP [41] to texts. For LVLMs, Parekh et al. [38] decompose the token representations to vision-language concepts. SAE-V [35] leverages a sparse autoencoder to token representations for efficient data sampling. Our method falls within the representation-based category. In contrast to existing methods that solely focus on

the vision or language representations, our VL-SAE investigates the alignment of vision-language representations by separately mapping their semantics into a unified concept set.

### 3 Methodology

We first introduce the architecture of current VLMs [41, 34, 1] and SAE [8, 32] (Section 3.1). Then, we perform the VLM alignment in an explicit form (Section 3.2). Finally, we propose the VL-SAE to map the semantics of vision-language representations into a unified concept set (Section 3.3).

#### 3.1 Preliminaries

**Contrastive Vision Language Models (CVLMs).** Existing CVLMs [41, 43] typically consist of a vision encoder and a language encoder. Given an input image and text, these encoders independently compute their respective representations. The semantic similarity between the image and text is then estimated through the cosine similarity between their corresponding representations. By collecting a large number of image-text pairs, CVLMs achieve the vision-language alignment by maximizing the representation similarity between semantically similar image-text pairs.

**Large Vision Language Models (LVLMs).** A general LVLM architecture [34, 27, 1] includes a vision encoder, an LLM, and a connector. An input image is first encoded through the vision encoder and then transformed into image tokens via the connector. Subsequently, these image tokens are concatenated with text tokens and provided as input to the LLM for text generation. With the image-text pairs, the vision-language representations of LVLMs are aligned by pre-training the model to generate textual answers for the text question related to the image content.

To conduct a uniform analysis of both types of models, we utilize the outputs of the vision and language encoders in CVLM for analysis. For LVLM, representations of the image and text tokens in the LLM’s hidden layer are averaged across the token axis for analysis. For convenience, we utilize  $\mathbf{x}_v, \mathbf{x}_l \in \mathbb{R}^d$  to uniformly represent the vision-language representations of CVLM and LVLM.

**Sparse Autoencoder (SAE).** SAE is an autoencoder with sparsity constraints on its hidden activations. Given an input  $\mathbf{x} \in \mathbb{R}^d$ , SAE first transforms it to hidden activations  $\mathbf{h} \in \mathbb{R}^h$  using an encoder  $E : \mathbb{R}^d \rightarrow \mathbb{R}^h$ , and then maps it back to the representation space via a decoder  $D : \mathbb{R}^h \rightarrow \mathbb{R}^d$ ,

$$\hat{\mathbf{x}} = D(\mathbf{h}) = D(\sigma(E(\mathbf{x}))), \quad (1)$$

where  $\sigma : \mathbb{R}^h \rightarrow \mathbb{R}^h$  denotes the sparsification function. SAE is trained with the reconstruction loss  $\|\hat{\mathbf{x}} - \mathbf{x}\|_2^2$  in a self-supervised manner. For sparsity constraints, previous methods usually select ReLU as the sparsification function  $\sigma$  and integrate the  $l_1$  norm of  $\mathbf{h}$  into the loss function [8]. Recently, researchers have found that directly adopting the top-k operation as the sparsification function not only eliminates the need for an additional loss term but also demonstrates superior scalability [15, 46].

#### 3.2 Explicit Representation Alignment

To ensure the activation consistency among semantically similar vision-language representations for alleviating the concept mismatch, a prerequisite is measuring the semantic similarity of representations from both modalities. For semantic similarity measurement, more semantically similar vision-language representations have higher cosine similarity in CVLMs [41, 43], which is explicitly constrained via the pre-training objective. However, it is difficult to measure the semantic similarity of LVLM representations [34, 1] due to their implicit alignment mechanism [50]. To address this problem, we propose employing an auxiliary autoencoder to convert the implicit alignment mechanism into an explicit alignment mechanism. Specifically, given an image-text pair, we input them into the VLM to extract representations  $(\mathbf{x}_v, \mathbf{x}_l)$ . The autoencoder transforms these representations into intermediate representations  $\mathbf{x}_v^e, \mathbf{x}_l^e \in \mathbb{R}^d$  via encoders  $\{E_v, E_l\}$  and then maps them back into the original representations  $\hat{\mathbf{x}}_v, \hat{\mathbf{x}}_l \in \mathbb{R}^d$  via decoders  $\{D_v, D_l\}$ ,

$$\hat{\mathbf{x}}_v = D_v(\mathbf{x}_v^e) = D_v(E_v(\mathbf{x}_v)), \quad \hat{\mathbf{x}}_l = D_l(\mathbf{x}_l^e) = D_l(E_l(\mathbf{x}_l)). \quad (2)$$

With the contrastive loss InfoNCE [41] and the reconstruction loss, the intermediate representations of image-text pairs can be aligned in cosine similarity while preserving the information of the original representations (details of InfoNCE are provided in Appendix A),

$$\mathcal{L}(\mathbf{x}_v, \mathbf{x}_l) = \text{InfoNCE}(\mathbf{x}_v^e, \mathbf{x}_l^e, \mathbf{x}_v^{e-}, \mathbf{x}_l^{e-}) + \|\hat{\mathbf{x}}_v - \mathbf{x}_v\|_2^2 + \|\hat{\mathbf{x}}_l - \mathbf{x}_l\|_2^2, \quad (3)$$

where  $\mathbf{x}_v^{e-}, \mathbf{x}_l^{e-}$  denote the intermediate representations of negative samples with dissimilar semantics from the given image-text pair. With this autoencoder, we can transform implicitly aligned representations into explicitly aligned intermediate representations, enabling the measurement of semantic similarity between vision and language representations. Note that this component is only utilized for LVLMs with the implicit alignment mechanism. For CVLMs with the explicit alignment mechanism, we directly use their original representations  $\mathbf{x}_v^e = \mathbf{x}_v, \mathbf{x}_l^e = \mathbf{x}_l$  for interpretation.

### 3.3 Interpreting Vision-Language Representations with a Unified Concept Set

Based on explicitly aligned representations, we propose the VL-SAE with a distance-based encoder and two modality-specific decoders to ensure the activation consistency of semantically similar representations, thereby alleviating the concept mismatch and interpreting multi-modal representations with a unified concept set.

**Encoder.** As the vision-language representations are aligned through cosine similarity, we propose an encoder that activates neurons based on the cosine similarity between the corresponding learnable weight vectors and the input representations. However, since cosine similarity does not satisfy the triangle inequality, two representations with high cosine similarity may not exhibit consistent similarity with the same weight vector, which hinders their activation consistency. To address this problem, we design a distance  $g : \mathbb{R}^d \times \mathbb{R}^d \rightarrow [0, 2]$  that utilizes the Euclidean distance between normalized inputs. Given the representation  $\mathbf{x}^e \in \mathbb{R}^d$  and weight vector  $\mathbf{w}_i \in \mathbb{R}^d$  corresponding to the  $i$ -th hidden neuron, their distance is calculated by

$$g(\mathbf{x}^e, \mathbf{w}_i) = \left\| \frac{\mathbf{x}^e}{\|\mathbf{x}^e\|_2} - \frac{\mathbf{w}_i}{\|\mathbf{w}_i\|_2} \right\|_2 = \sqrt{2 - 2\cos(\mathbf{x}^e, \mathbf{w}_i)}, \quad (4)$$

where  $\cos(\mathbf{x}^e, \mathbf{w}_i)$  denotes the cosine similarity of  $\mathbf{x}^e$  and  $\mathbf{w}_i$ . Since the distance  $g$  is a variant of the Euclidean distance, it naturally satisfies the triangle inequality. This indicates that the difference in distance values between the weight vector  $\mathbf{w}_i$  and vision-language representations  $\mathbf{x}_v^e, \mathbf{x}_l^e$  cannot exceed the distance between the two representations,

$$|g(\mathbf{x}_v^e, \mathbf{w}_i) - g(\mathbf{x}_l^e, \mathbf{w}_i)| \leq g(\mathbf{x}_v^e, \mathbf{x}_l^e). \quad (5)$$

The proposed metric exhibits a negative correlation with cosine similarity, suggesting that as the cosine similarity of vision-language representation increases, the upper bound of the difference in their activations decreases accordingly. We utilize the negative value of  $g$  as the activation value, thereby ensuring the positive correlation between the activation value and cosine similarity.

$$E^s(\mathbf{x}^e)[i] = 2 - g(\mathbf{x}^e, \mathbf{w}_i) = 2 - \sqrt{2 - 2\cos(\mathbf{x}^e, \mathbf{w}_i)}, \quad (6)$$

where  $E^s(\mathbf{x}^e)[i]$  denotes the  $i$ -th value of  $E^s(\mathbf{x}^e) \in \mathbb{R}^h$ . We introduce a constant 2 to ensure the non-negativity of the activation values. For the sparsification function  $\sigma$ , we employ the top-k function (*i.e.*, retaining top-k largest values while setting others to zero) considering its strong scalability [15, 47, 48],

$$\mathbf{h} = \text{TopK}(E^s(\mathbf{x}^e)). \quad (7)$$

The number of activated neurons  $k$  serves as a hyper-parameter. This distance-based encoder bounds the activation discrepancy of semantically similar representations through the triangle inequality, promoting each neuron to be co-activated by semantically similar images and texts.

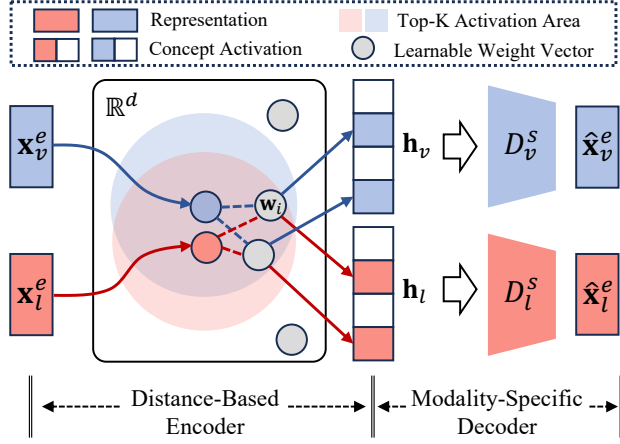


Figure 2: VL-SAE consists of a distance-based encoder that maps semantically similar **vision-language** representations to similar activations, and two modality-specific decoders that reconstruct original representations from these activations.

Given the representation  $\mathbf{x}^e \in \mathbb{R}^d$  and weight vector  $\mathbf{w}_i \in \mathbb{R}^d$  corresponding to the  $i$ -th hidden neuron, their distance is calculated by

$$g(\mathbf{x}^e, \mathbf{w}_i) = \left\| \frac{\mathbf{x}^e}{\|\mathbf{x}^e\|_2} - \frac{\mathbf{w}_i}{\|\mathbf{w}_i\|_2} \right\|_2 = \sqrt{2 - 2\cos(\mathbf{x}^e, \mathbf{w}_i)}, \quad (4)$$

where  $\cos(\mathbf{x}^e, \mathbf{w}_i)$  denotes the cosine similarity of  $\mathbf{x}^e$  and  $\mathbf{w}_i$ . Since the distance  $g$  is a variant of the Euclidean distance, it naturally satisfies the triangle inequality. This indicates that the difference in distance values between the weight vector  $\mathbf{w}_i$  and vision-language representations  $\mathbf{x}_v^e, \mathbf{x}_l^e$  cannot exceed the distance between the two representations,

$$|g(\mathbf{x}_v^e, \mathbf{w}_i) - g(\mathbf{x}_l^e, \mathbf{w}_i)| \leq g(\mathbf{x}_v^e, \mathbf{x}_l^e). \quad (5)$$

The proposed metric exhibits a negative correlation with cosine similarity, suggesting that as the cosine similarity of vision-language representation increases, the upper bound of the difference in their activations decreases accordingly. We utilize the negative value of  $g$  as the activation value, thereby ensuring the positive correlation between the activation value and cosine similarity.

$$E^s(\mathbf{x}^e)[i] = 2 - g(\mathbf{x}^e, \mathbf{w}_i) = 2 - \sqrt{2 - 2\cos(\mathbf{x}^e, \mathbf{w}_i)}, \quad (6)$$

where  $E^s(\mathbf{x}^e)[i]$  denotes the  $i$ -th value of  $E^s(\mathbf{x}^e) \in \mathbb{R}^h$ . We introduce a constant 2 to ensure the non-negativity of the activation values. For the sparsification function  $\sigma$ , we employ the top-k function (*i.e.*, retaining top-k largest values while setting others to zero) considering its strong scalability [15, 47, 48],

$$\mathbf{h} = \text{TopK}(E^s(\mathbf{x}^e)). \quad (7)$$

The number of activated neurons  $k$  serves as a hyper-parameter. This distance-based encoder bounds the activation discrepancy of semantically similar representations through the triangle inequality, promoting each neuron to be co-activated by semantically similar images and texts.

**Decoder.** Despite bounding the activation discrepancy of vision-language representations through the distance-based encoder, it remains insufficient for interpreting representations from distinct distributions. This is because the decoder reconstructs representations solely based on hidden activations. Reconstructing vision-language representations with the same decoder leads to the incorporation of distributional information into the hidden activations during training, thereby reducing the activation consistency of vision-language representations that have similar semantics.

To map the hidden activations into representations of distinct distributions, we propose employing separate decoders for each modality. Given the activations  $\mathbf{h}_v, \mathbf{h}_l \in \mathbb{R}^h$  of vision and language representations  $\mathbf{x}_v^e, \mathbf{x}_l^e \in \mathbb{R}^d$ , two modality-specific decoders  $D_v^s, D_l^s$  are utilized to transform these activations back to their original representations, respectively,

$$\hat{\mathbf{x}}_v^e = D_v^s(\mathbf{h}_v), \hat{\mathbf{x}}_l^e = D_l^s(\mathbf{h}_l). \quad (8)$$

VL-SAE is trained through the reconstruction loss of visual-language representations,

$$\mathcal{L}(\mathbf{x}_v^e, \mathbf{x}_l^e) = \|\hat{\mathbf{x}}_v^e - \mathbf{x}_v^e\|_2^2 + \|\hat{\mathbf{x}}_l^e - \mathbf{x}_l^e\|_2^2. \quad (9)$$

With the separate decoders for storing distributional information, VL-SAE can encode semantically similar vision-language representations to consistent concept activations as interpretations, and then map these activations back to representations of distinct distributions.

## 4 Experiments

In experiments, we first provide the implementation details for constructing VL-SAE based on VLM representations in Section 4.1. Next, we evaluate the concepts learned by VL-SAE in Section 4.2. Finally, we integrate VL-SAE into the inference process of pre-trained VLMs to interpret and enhance their vision-language alignment mechanisms in Section 4.3.

### 4.1 Implementation Details for VL-SAE Construction.

**VLM Selection.** To demonstrate the broad applicability of the proposed VL-SAE, we build it upon multiple representative VLMs, including CVLMs (OpenCLIP [43] with ViT-B/32, ViT-B/16, ViT-L/14, ViT-H/14) pre-trained with retrieval tasks, and LVLMs (LLaVA1.5 [34], Qwen-VL [1]) pre-trained with question answering tasks. For CVLMs, VL-SAE is constructed using the output from both their vision and language encoders. For LVLMs, VL-SAE is constructed using the output features of the LLM hidden layers (the 29-th layer of LLaVA1.5 and the 26-th layer of Qwen-VL).

**Datasets.** We fed the CC3M dataset [45] containing 3 million image-text pairs into the VLM to extract the corresponding vision-language representations. These representations are randomly divided into training and test sets at a ratio of 4:1.

**Training Strategies.** For LVLMs [34, 1], we first train the auxiliary autoencoder for 50 epochs to perform the explicit representation alignment. The training process is configured with a batch size of 2048, a weight decay of 0.01, and a learning rate of 5e-5. Then, the VL-SAE is trained for 10 epochs based on the intermediate representations of the autoencoder with a batch size of 512 and a learning rate of 1e-4. For CVLMs [43], we adopt the same strategy as the LVLMs but omit the training of the auxiliary autoencoder because CVLM representations are naturally aligned through cosine similarity.

### 4.2 Evaluating the Quality of VL-SAE Concept Set

**Quantitative Evaluation.** For the concept set, we evaluate (i) whether each neuron is activated by semantically similar images and texts, and (ii) whether diverse semantic concepts are learned across different neurons. These two aspects are quantitatively assessed using the CLIP score [41]. Specifically, we first gather the maximally activating images and texts for each neuron of the VL-SAE’s hidden layer to describe its semantics. Then, the CLIP score is employed to quantify the semantic similarity between images and texts within the same neuron (Intra-Similarity) and across different neurons (Inter-Similarity). The Intra-Similarity evaluates the semantic consistency of images and texts within each concept, while the Inter-Similarity assesses the semantic diversity across the concept set. Detailed descriptions of both metrics are presented in Appendix A.1.

For comparison, we consider two baselines using current SAE architectures (i) SAE-D, which employs distinct SAEs for vision and language representations, and (ii) SAE-S, which uses a single

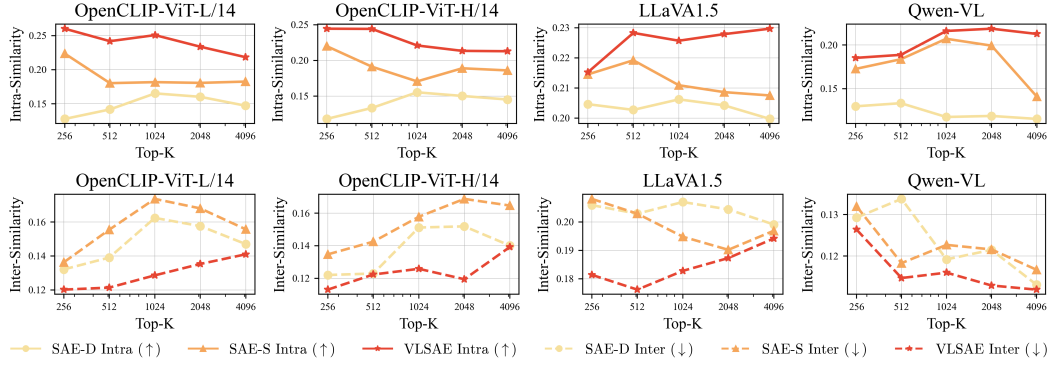


Figure 3: Quantitative evaluation of the learned concept set. We compare the VL-SAE with other methods on the consistency between vision and language semantics within the same neuron (Intra-Similarity) and the semantic diversity across different neurons (Inter-Similarity) on multiple VLMs.

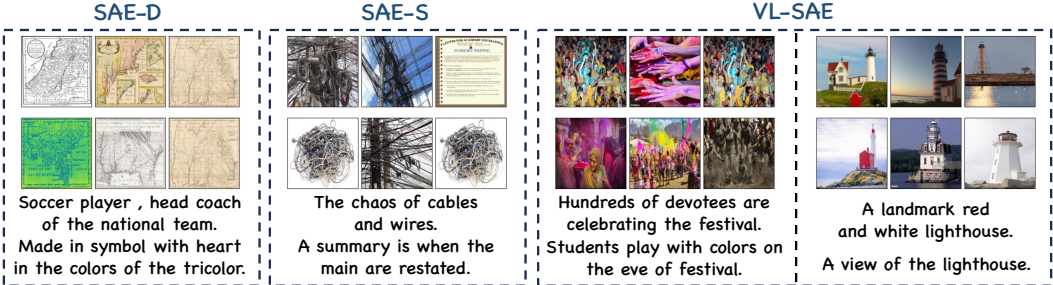


Figure 4: Qualitative comparisons among concepts of SAE-D, SAE-S and the proposed VL-SAE. All SAEs are trained with the vision-language representations of LLaVA 1.5.

SAE shared by both modalities. As shown in Figure 3, VL-SAE exhibits higher intra-similarity and lower inter-similarity compared to these methods, consistently across various VLMs and different numbers of activated concepts. This suggests that *the concepts learned by VL-SAE possess more consistent vision-language semantics and richer semantic diversity than current methods*.

**Qualitative Evaluation.** We provide qualitative comparisons among SAE-D, SAE-S, and our VL-SAE in Figure 4. SAE-D, which employs separate SAEs for each modality, can extract concepts with consistent semantics within the same modality but encounters the concept mismatch issue as illustrated in Figure 1(b). SAE-S, which utilizes a shared SAE for both modalities, demonstrates a less significant concept mismatch compared to SAE-D. However, semantic inconsistencies still exist, such as the conflation of the semantics of "wire" and "summary tutorials" under a single concept. In contrast, the concepts in VL-SAE consist of samples with consistently aligned semantics.

### 4.3 Interpreting and Enhancing the Vision-Language Alignment

With the VL-SAE that correlates the semantics of vision and language representations with a unified concept set, we can interpret and enhance the vision-language alignment mechanism in CVLMs and LVLMs by comparing the semantics of both modalities using the concept set.

**Interpreting Vision-Language Alignment of CVLMs.** Given an image-text pair, we separately map the corresponding vision and language representations into the unified concept set through VL-SAE. Figure 5 depicts several examples by visualizing the concepts activated by representations for each modality and the aligned concepts that are co-activated by both modalities. We observe that (i) single-modal representations can activate concepts with irrelevant semantics (*e.g.*, the representations of a motorcycle image activate the concept of a car). This phenomenon reveals the mismatch between representation similarity and semantic similarity in single-modal samples, which arises due to contrastive learning's inability to effectively model the relationships among representations within the same modality. (ii) The aligned concepts exhibit strong semantic similarity to both the given image and text, suggesting that the irrelevant concepts activated by a single-modal representation are not simultaneously activated by representations of the other modality.



Figure 5: Interpreting the vision-language alignment of OpenCLIP-ViT-L/14 with VL-SAE. Given an image-text pair, we visualize the concepts activated by corresponding **vision** and **language** representations separately, as well as the **aligned concepts** co-activated by both modalities. Concepts only related to single-modal representations are highlighted **in purple**.

Table 1: Performance of OpenCLIP with varying model sizes in zero-shot image classification tasks.

	Caltech101	Cifar10	Cifar100	Country211	DTD	Eurosat	Flowers	Food	GTSRB	MNIST	Pets	SST2	STL10	Sun397	Mean Acc.
ViT-B/32	86.5	93.6	75.5	16.7	55.9	47.2	71.6	82.7	49.3	69.8	90.7	57.5	96.6	68.7	68.7
+VL-SAE	86.7	93.8	75.7	16.7	56.9	51.0	71.8	82.8	50.3	71.8	90.7	57.9	96.9	69.4	<b>69.5</b>
ViT-B/16	86.7	94.9	76.9	20.3	56.5	52.6	71.4	86.6	46.1	66.0	90.3	59.7	97.9	70.8	69.8
+VL-SAE	87.2	95.1	77.0	20.4	56.7	53.2	71.6	86.8	49.1	67.8	90.9	60.4	97.9	71.4	<b>70.4</b>
ViT-L/14	87.6	95.8	78.3	24.4	61.5	57.8	74.4	88.8	51.6	64.5	92.9	60.3	98.5	74.0	72.2
+VL-SAE	87.9	95.9	78.6	24.5	62.8	60.3	74.5	88.8	51.9	69.1	93.0	60.6	98.6	74.3	<b>72.9</b>
ViT-H/14	88.2	97.5	84.7	29.8	67.9	72.7	80.1	92.7	58.3	72.9	94.5	64.1	98.5	75.2	76.9
+VL-SAE	88.5	97.7	85.0	30.0	68.4	76.7	80.1	92.9	59.5	76.1	94.7	65.2	98.6	75.3	<b>77.8</b>

**Enhancing Vision-Language Alignment of CVLMs.** According to the above interpretations, mapping vision-language representations to a unified concept set enables filtering out the irrelevant concepts activated by single-modal representations. Inspired by this, we enhance the vision-language alignment of CVLMs by aligning their multi-modal representations in concepts. Specifically, for an input image  $x_v$  and text  $x_l$ , their semantic similarity depends not only on the cosine similarities of their representations  $\mathbf{x}_v, \mathbf{x}_l$ , but also on the cosine similarities of their concept activations  $\mathbf{h}_v, \mathbf{h}_l$ .

$$y = \cos(\mathbf{x}_v, \mathbf{x}_l) + \alpha_c \cos(\mathbf{h}_v, \mathbf{h}_l), \quad (10)$$

where  $\alpha_c$  is a task-specific hyperparameter that controls the proportion of concept-based predictions. We enhance the alignment mechanism of multiple CVLMs and conduct evaluations across various zero-shot image classification datasets [59, 25, 41, 6, 18, 36, 3, 19, 10, 39, 51, 7, 61]. As Table 1 shows, mapping multi-modal representations to a unified concept set for predictions achieves consistent performance improvement across different models and datasets.

**Interpreting Vision-Language Alignment of LVLMs.** For LVLMs, we interpret their alignment mechanism by visualizing the concepts activated by the vision and language representations during the text generation process. As Figure 6 shows, given the input image of a kitchen including ovens and stoves, the generated text exhibits object hallucinations of the microwave and refrigerator. By analyzing the activated concepts, we observe that the semantics of both vision and language representations are correlated with the kitchen scene but emphasize different objects. Specifically, the vision representation focuses on ovens and stoves, whereas the language representation is associated with microwaves and refrigerators, which correspond to the hallucinated objects. This phenomenon indicates that the object information in the vision representation is inadequately transferred into the language representation, resulting in hallucinations in the generated text.

**Enhancing Vision-Language Alignment of LVLMs.** As the hallucinations of LVLMs are correlated to the misalignment between vision and language representations, we leverage VL-SAE to mitigate

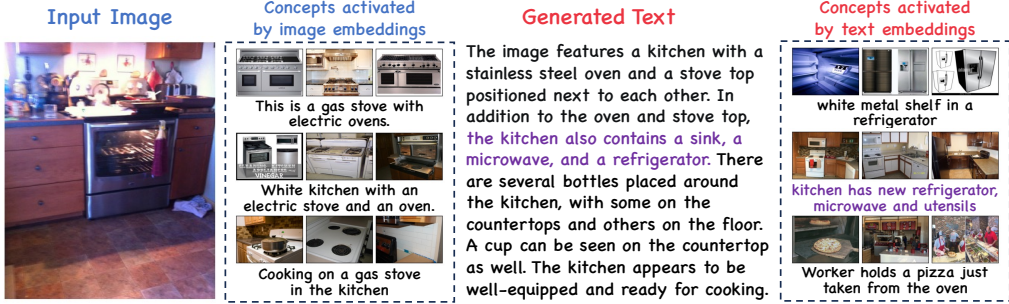


Figure 6: Interpreting the vision-language alignment of LLaVA1.5 with VL-SAE. Given an input image and the text generated by LLMs, we visualize the concepts activated by corresponding vision and language representations. The **hallucination concept** activated by language representations facilitates a deeper understanding of **object hallucinations in the text**.

Table 2: Experimental results on POPE for hallucination elimination.

Setting	Decoding	LLaVA1.5				Qwen-VL			
		Accuracy	Precision	Recall	F1 Score	Accuracy	Precision	Recall	F1 Score
Random	Regular	82.93	92.01	72.13	80.87	85.20	95.99	73.47	83.23
	VCD	85.53	93.68	76.20	84.04	86.33	96.11	<b>75.73</b>	84.71
	VL-SAE	<b>87.07</b>	<b>97.28</b>	<b>76.27</b>	<b>85.50</b>	<b>86.47</b>	<b>97.15</b>	75.13	<b>84.74</b>
Popular	Regular	81.13	87.96	72.13	79.27	83.80	94.47	71.80	81.59
	VCD	83.63	89.51	76.20	82.31	85.73	94.30	<b>76.10</b>	84.21
	VL-SAE	<b>85.87</b>	<b>94.39</b>	<b>76.27</b>	<b>84.37</b>	<b>85.97</b>	<b>96.15</b>	74.93	<b>84.22</b>
Adversarial	Regular	78.67	83.03	72.07	77.16	82.33	89.88	72.87	80.49
	VCD	81.10	84.47	<b>76.20</b>	80.13	83.77	90.03	<b>75.93</b>	82.39
	VL-SAE	<b>83.60</b>	<b>89.44</b>	<b>76.20</b>	<b>82.29</b>	<b>86.10</b>	<b>97.29</b>	74.26	<b>84.23</b>

hallucinations by enhancing the vision-language alignment at the concept level. Specifically, with the vision and language representations  $\mathbf{x}_v, \mathbf{x}_l$ , we obtain a refined language representation  $\hat{\mathbf{x}}_l$  by aligning its concept activation  $\mathbf{h}_l$  with vision concept activation  $\mathbf{h}_v$  through VL-SAE,

$$\hat{\mathbf{x}}_l = (1 - \alpha_l)\mathbf{x}_l + \alpha_l D_l(D_l^s(\mathbf{h}_l + \beta\mathbf{h}_v)). \quad (11)$$

The modified language representation  $\hat{\mathbf{x}}_l$  is utilized to mitigate hallucinations through contrastive decoding [26]. More implementation details are provided in Appendix A. Table 2 shows the performance comparisons on the POPE [30] benchmark. As a method for representation interpretation, VL-SAE surpasses the VCD [26] that specializes in hallucination elimination. The effectiveness of VL-SAE further highlights the potential of representation interpretation methods to improve model performance on downstream tasks by enhancing the vision-language alignment.

#### 4.4 Ablation Studies & Visualizations

**Effects of the VL-SAE Architecture.** The ablation studies of the proposed components are provided in Table 3. First, replacing the standard encoder with the cosine-based encoder (+Cosine-based Encoder), which activates hidden neurons based on cosine similarity, can improve the quality of learned concepts, as vision-language representations are explicitly aligned through cosine similarity.

Moreover, replacing the cosine similarity with the distance proposed in Equation 4 can improve the concept quality (+Distance-based Encoder). This is because the distance satisfies the triangle inequality, enabling each hidden neuron to be activated by more semantically similar visual-language representations. Additionally, the improvement achieved by adopting modality-

Table 3: Ablation studies of the proposed architecture.

	OpenCLIP-ViT-H/14		LLaVA1.5	
	Intra-Sim. ( $\uparrow$ )	Inter-Sim. ( $\downarrow$ )	Intra-Sim. ( $\uparrow$ )	Inter-Sim. ( $\downarrow$ )
Standard SAE	0.1890	0.1688	0.2086	0.1902
+Auxiliary Autoencoder	-	-	0.2092	0.1908
+Cosine-based Encoder	0.1891	0.1518	0.2103	0.1902
+Distance-based Encoder	0.2016	0.1357	0.2216	0.1842
+Modality-specific Decoder	<b>0.2134</b>	<b>0.1149</b>	<b>0.2257</b>	<b>0.1828</b>
-Auxiliary Autoencoder	-	-	0.2084	0.2034

Table 4: Concept quality of VL-SAE pre-trained with different proportions of the CC3M dataset.

Data Percentage	10%	30%	50%	70%	100%
Intra-Similarity ( $\uparrow$ )	0.2029	0.2129	0.2196	0.2222	<b>0.2299</b>
Inter-Similarity ( $\downarrow$ )	0.1597	0.1306	0.126	0.1256	<b>0.1220</b>

Table 5: Ablation studies of the sparsification method in VL-SAE.

Method	Intra-Similarity ( $\uparrow$ )	Inter-Similarity ( $\downarrow$ )
L1	0.2142	0.1809
Top-K	<b>0.2442</b>	<b>0.1373</b>



Figure 7: Qualitative evaluation of the learned concept set. We provide the maximally activating images and texts for several concepts of VL-SAE trained with the representations of LLaVA 1.5.

specific decoders stems from mitigating the adverse influence of distributional discrepancies in multi-modal representations on the encoder. Furthermore, directly training the VL-SAE with original representations of LVLMs (-Auxiliary Autoencoder) causes the failure of other components, highlighting the necessity of transforming the alignment mechanism to an explicit form.

**Effects of the Dataset Volume.** In Table 4, we train VL-SAE models with different proportions of the CC3M dataset and report their Intra-Similarity and Inter-Similarity. As the volume of data increases, the Intra-Similarity (0.2029 $\rightarrow$ 0.2299) and Inter-Similarity (0.1597 $\rightarrow$ 0.1220) of the concepts learned by VL-SAE improve accordingly. This suggests that VL-SAE can learn higher-quality concepts by leveraging larger amounts of data in a self-supervised manner.

**Effects of the Sparsification Method.** In Table 5, we compare the performance of utilizing Top-k [47, 46] and L1 loss [8] for sparsification. The coefficient of L1 loss is set to 1e-4. We find that employing Top-K sparsification yields superior concept quality compared to L1 loss, as the latter lacks precise control over the number of activated hidden neurons. This limitation hinders its ability to effectively balance sparsity in neuron activation with the self-supervised representation reconstruction loss. Our results are consistent with previous studies [15], which also indicate that Top-K sparsification is a more effective and scalable approach.

**Visualizations of Concepts Learned by VL-SAE.** In Figure 7, we visualize the learned concepts of VL-SAE, which are represented by their maximally activating images and texts. The images and texts of the same concept exhibit highly similar semantics, demonstrating that VL-SAE can effectively alleviate the concept mismatch. Additionally, VL-SAE obtains concepts with abstract semantics rather than focusing exclusively on semantics related to visual appearance. For example, concept 5478 is style-agnostic and activated by both natural and cartoon images, which depict humans lying on a beach. Concept 7301 is color-agnostic and activated by images of happy new year posters.

## 5 Conclusion

In this work, we map the semantics of vision-language representations into a unified concept set with VL-SAE, which is trained by encouraging the consistency of its hidden activations among semantically similar representations under self-supervision. To measure the semantic similarity of multi-modal representations, we perform their alignment in an explicit form that correlates the semantic similarity with cosine similarity. To ensure the activation consistency among semantically similar representations, we propose the VL-SAE architecture, including a distance-based encoder and two modality-specific decoders. Experimental results demonstrate the superior ability of VL-SAE to interpret and enhance the alignment mechanism of VLMs. For future work, we will apply the proposed method to more VLMs and investigate its capabilities in additional tasks such as model unlearning and continuous learning. For limitations discussion, please refer to Appendix C.4.

## Acknowledgement and Disclosure of Funding

This work was supported in part by the National Key R&D Program of China under Grant 2023YFC2508704, in part by the National Natural Science Foundation of China 62236008, and in part by the Fundamental Research Funds for the Central Universities. The authors would like to thank Siqi Zhang, Yue Wu, and the anonymous reviewers for their constructive comments and suggestions that improved this manuscript.

## References

- [1] Jinze Bai, Shuai Bai, Shusheng Yang, Shijie Wang, Sinan Tan, Peng Wang, Junyang Lin, Chang Zhou, and Jingren Zhou. Qwen-vl: A versatile vision-language model for understanding, localization, text reading, and beyond, 2023.
- [2] Usha Bhalla, Alex Oesterling, Suraj Srinivas, Flávio P. Calmon, and Himabindu Lakkaraju. Interpreting CLIP with sparse linear concept embeddings (splice). In Amir Globersons, Lester Mackey, Danielle Belgrave, Angela Fan, Ulrich Paquet, Jakub M. Tomczak, and Cheng Zhang, editors, *Advances in Neural Information Processing Systems 38: Annual Conference on Neural Information Processing Systems 2024, NeurIPS 2024, Vancouver, BC, Canada, December 10 - 15, 2024*, 2024.
- [3] Lukas Bossard, Matthieu Guillaumin, and Luc Van Gool. Food-101—mining discriminative components with random forests. In *Computer vision—ECCV 2014: 13th European conference, zurich, Switzerland, September 6–12, 2014, proceedings, part VI 13*, pages 446–461. Springer, 2014.
- [4] Hila Chefer, Shir Gur, and Lior Wolf. Generic attention-model explainability for interpreting bi-modal and encoder-decoder transformers. In *Proceedings of the IEEE/CVF international conference on computer vision*, pages 397–406, 2021.
- [5] Junxi Chen, Liang Li, Yunbin Tu, Li Su, Zhe Xue, and Qingming Huang. Generalizing single-frame supervision to event-level understanding for video anomaly detection. In *The Thirty-ninth Annual Conference on Neural Information Processing Systems*.
- [6] Mircea Cimpoi, Subhransu Maji, Iasonas Kokkinos, Sammy Mohamed, and Andrea Vedaldi. Describing textures in the wild. In *2014 IEEE Conference on Computer Vision and Pattern Recognition, CVPR 2014, Columbus, OH, USA, June 23-28, 2014*, pages 3606–3613. IEEE Computer Society, 2014.
- [7] Adam Coates, Andrew Ng, and Honglak Lee. An analysis of single-layer networks in unsupervised feature learning. In *Proceedings of the fourteenth international conference on artificial intelligence and statistics*, pages 215–223. JMLR Workshop and Conference Proceedings, 2011.
- [8] Hoagy Cunningham, Aidan Ewart, Logan Riggs, Robert Huben, and Lee Sharkey. Sparse autoencoders find highly interpretable features in language models. *ArXiv preprint*, abs/2309.08600, 2023.
- [9] Yunkai Dang, Kaichen Huang, Jiahao Huo, Yibo Yan, Sirui Huang, Dongrui Liu, Mengxi Gao, Jie Zhang, Chen Qian, Kun Wang, et al. Explainable and interpretable multimodal large language models: A comprehensive survey. *ArXiv preprint*, abs/2412.02104, 2024.
- [10] Li Deng. The mnist database of handwritten digit images for machine learning research [best of the web]. *IEEE signal processing magazine*, 29(6):141–142, 2012.
- [11] Xin Dong, Shangyu Chen, and Sinno Jialin Pan. Learning to prune deep neural networks via layer-wise optimal brain surgeon. In Isabelle Guyon, Ulrike von Luxburg, Samy Bengio, Hanna M. Wallach, Rob Fergus, S. V. N. Vishwanathan, and Roman Garnett, editors, *Advances in Neural Information Processing Systems 30: Annual Conference on Neural Information Processing Systems 2017, December 4-9, 2017, Long Beach, CA, USA*, pages 4857–4867, 2017.

[12] Alexey Dosovitskiy, Lucas Beyer, Alexander Kolesnikov, Dirk Weissenborn, Xiaohua Zhai, Thomas Unterthiner, Mostafa Dehghani, Matthias Minderer, Georg Heigold, Sylvain Gelly, Jakob Uszkoreit, and Neil Houlsby. An image is worth 16x16 words: Transformers for image recognition at scale. In *9th International Conference on Learning Representations, ICLR 2021, Virtual Event, Austria, May 3-7, 2021*. OpenReview.net, 2021.

[13] Jiali Duan, Liqun Chen, Son Tran, Jinyu Yang, Yi Xu, Belinda Zeng, and Trishul Chilimbi. Multi-modal alignment using representation codebook. In *IEEE/CVF Conference on Computer Vision and Pattern Recognition, CVPR 2022, New Orleans, LA, USA, June 18-24, 2022*, pages 15630–15639. IEEE, 2022.

[14] Yossi Gandelsman, Alexei A Efros, and Jacob Steinhardt. Interpreting clip’s image representation via text-based decomposition. *ArXiv preprint*, abs/2310.05916, 2023.

[15] Leo Gao, Tom Dupré la Tour, Henk Tillman, Gabriel Goh, Rajan Troll, Alec Radford, Ilya Sutskever, Jan Leike, and Jeffrey Wu. Scaling and evaluating sparse autoencoders. *ArXiv preprint*, abs/2406.04093, 2024.

[16] Gabriel Goh, Nick Cammarata, Chelsea Voss, Shan Carter, Michael Petrov, Ludwig Schubert, Alec Radford, and Chris Olah. Multimodal neurons in artificial neural networks. *Distill*, 6(3):e30, 2021.

[17] Aaron Grattafiori, Abhimanyu Dubey, Abhinav Jauhri, Abhinav Pandey, Abhishek Kadian, Ahmad Al-Dahle, Aiesha Letman, Akhil Mathur, Alan Schelten, Alex Vaughan, et al. The llama 3 herd of models. *ArXiv preprint*, abs/2407.21783, 2024.

[18] Patrick Helber, Benjamin Bischke, Andreas Dengel, and Damian Borth. Eurosat: A novel dataset and deep learning benchmark for land use and land cover classification. *IEEE Journal of Selected Topics in Applied Earth Observations and Remote Sensing*, 12(7):2217–2226, 2019.

[19] Sebastian Houben, Johannes Stallkamp, Jan Salmen, Marc Schlipsing, and Christian Igel. Detection of traffic signs in real-world images: The german traffic sign detection benchmark. In *The 2013 international joint conference on neural networks (IJCNN)*, pages 1–8. Ieee, 2013.

[20] Edward J. Hu, Yelong Shen, Phillip Wallis, Zeyuan Allen-Zhu, Yuanzhi Li, Shean Wang, Lu Wang, and Weizhu Chen. Lora: Low-rank adaptation of large language models. In *The Tenth International Conference on Learning Representations, ICLR 2022, Virtual Event, April 25-29, 2022*. OpenReview.net, 2022.

[21] Qidong Huang, Xiaoyi Dong, Pan Zhang, Bin Wang, Conghui He, Jiaqi Wang, Duhua Lin, Weiming Zhang, and Nenghai Yu. Opera: Alleviating hallucination in multi-modal large language models via over-trust penalty and retrospection-allocation. In *Proceedings of the IEEE/CVF Conference on Computer Vision and Pattern Recognition*, pages 13418–13427, 2024.

[22] Chao Jia, Yinfai Yang, Ye Xia, Yi-Ting Chen, Zarana Parekh, Hieu Pham, Quoc V. Le, Yun-Hsuan Sung, Zhen Li, and Tom Duerig. Scaling up visual and vision-language representation learning with noisy text supervision. In Marina Meila and Tong Zhang, editors, *Proceedings of the 38th International Conference on Machine Learning, ICML 2021, 18-24 July 2021, Virtual Event*, volume 139 of *Proceedings of Machine Learning Research*, pages 4904–4916. PMLR, 2021.

[23] Mingyu Jin, Qinkai Yu, Jingyuan Huang, Qingcheng Zeng, Zhenting Wang, Wenyue Hua, Haiyan Zhao, Kai Mei, Yanda Meng, Kaize Ding, et al. Exploring concept depth: How large language models acquire knowledge and concept at different layers? *ArXiv preprint*, abs/2404.07066, 2024.

[24] Been Kim, Martin Wattenberg, Justin Gilmer, Carrie J. Cai, James Wexler, Fernanda B. Viégas, and Rory Sayres. Interpretability beyond feature attribution: Quantitative testing with concept activation vectors (TCAV). In Jennifer G. Dy and Andreas Krause, editors, *Proceedings of the 35th International Conference on Machine Learning, ICML 2018, Stockholmsmässan, Stockholm, Sweden, July 10-15, 2018*, volume 80 of *Proceedings of Machine Learning Research*, pages 2673–2682. PMLR, 2018.

[25] Alex Krizhevsky, Geoffrey Hinton, et al. Learning multiple layers of features from tiny images. 2009.

[26] Sicong Leng, Hang Zhang, Guanzheng Chen, Xin Li, Shijian Lu, Chunyan Miao, and Lidong Bing. Mitigating object hallucinations in large vision-language models through visual contrastive decoding. In *Proceedings of the IEEE/CVF Conference on Computer Vision and Pattern Recognition*, pages 13872–13882, 2024.

[27] Junnan Li, Dongxu Li, Silvio Savarese, and Steven C. H. Hoi. BLIP-2: bootstrapping language-image pre-training with frozen image encoders and large language models. In Andreas Krause, Emma Brunskill, Kyunghyun Cho, Barbara Engelhardt, Sivan Sabato, and Jonathan Scarlett, editors, *International Conference on Machine Learning, ICML 2023, 23-29 July 2023, Honolulu, Hawaii, USA*, volume 202 of *Proceedings of Machine Learning Research*, pages 19730–19742. PMLR, 2023.

[28] Qing Li, Jiahui Geng, Derui Zhu, Fengyu Cai, Chenyang Lyu, and Fakhri Karray. Sauce: Selective concept unlearning in vision-language models with sparse autoencoders. *ArXiv preprint*, abs/2503.14530, 2025.

[29] Xiang Lisa Li, Ari Holtzman, Daniel Fried, Percy Liang, Jason Eisner, Tatsunori Hashimoto, Luke Zettlemoyer, and Mike Lewis. Contrastive decoding: Open-ended text generation as optimization. In Anna Rogers, Jordan Boyd-Graber, and Naoaki Okazaki, editors, *Proceedings of the 61st Annual Meeting of the Association for Computational Linguistics (Volume 1: Long Papers)*, pages 12286–12312, Toronto, Canada, 2023. Association for Computational Linguistics.

[30] Yifan Li, Yifan Du, Kun Zhou, Jinpeng Wang, Xin Zhao, and Ji-Rong Wen. Evaluating object hallucination in large vision-language models. In Houda Bouamor, Juan Pino, and Kalika Bali, editors, *Proceedings of the 2023 Conference on Empirical Methods in Natural Language Processing*, pages 292–305, Singapore, 2023. Association for Computational Linguistics.

[31] Dongze Lian, Daquan Zhou, Jiashi Feng, and Xinchao Wang. Scaling & shifting your features: A new baseline for efficient model tuning. In Sanmi Koyejo, S. Mohamed, A. Agarwal, Danielle Belgrave, K. Cho, and A. Oh, editors, *Advances in Neural Information Processing Systems 35: Annual Conference on Neural Information Processing Systems 2022, NeurIPS 2022, New Orleans, LA, USA, November 28 - December 9, 2022*, 2022.

[32] Hyesu Lim, Jinho Choi, Jaegul Choo, and Steffen Schneider. Sparse autoencoders reveal selective remapping of visual concepts during adaptation. *ArXiv preprint*, abs/2412.05276, 2024.

[33] Hanchao Liu, Wenyuan Xue, Yifei Chen, Dapeng Chen, Xiutian Zhao, Ke Wang, Liping Hou, Rongjun Li, and Wei Peng. A survey on hallucination in large vision-language models. *ArXiv preprint*, abs/2402.00253, 2024.

[34] Haotian Liu, Chunyuan Li, Qingyang Wu, and Yong Jae Lee. Visual instruction tuning. In Alice Oh, Tristan Naumann, Amir Globerson, Kate Saenko, Moritz Hardt, and Sergey Levine, editors, *Advances in Neural Information Processing Systems 36: Annual Conference on Neural Information Processing Systems 2023, NeurIPS 2023, New Orleans, LA, USA, December 10 - 16, 2023*, 2023.

[35] Hantao Lou, Changye Li, Jiaming Ji, and Yaodong Yang. Sae-v: Interpreting multimodal models for enhanced alignment. *ArXiv preprint*, abs/2502.17514, 2025.

[36] Maria-Elena Nilsback and Andrew Zisserman. Automated flower classification over a large number of classes. In *Sixth Indian Conference on Computer Vision, Graphics & Image Processing, ICVGIP 2008, Bhubaneswar, India, 16-19 December 2008*, pages 722–729. IEEE Computer Society, 2008.

[37] Haowen Pan, Yixin Cao, Xiaozhi Wang, Xun Yang, and Meng Wang. Finding and editing multi-modal neurons in pre-trained transformers. *ArXiv preprint*, abs/2311.07470, 2023.

[38] Jayneel Parekh, Pegah Khayatan, Mustafa Shukor, Alasdair Newson, and Matthieu Cord. A concept-based explainability framework for large multimodal models. In Amir Globersons, Lester Mackey, Danielle Belgrave, Angela Fan, Ulrich Paquet, Jakub M. Tomczak, and Cheng Zhang, editors, *Advances in Neural Information Processing Systems 38: Annual Conference on Neural Information Processing Systems 2024, NeurIPS 2024, Vancouver, BC, Canada, December 10 - 15, 2024*, 2024.

[39] Omkar M. Parkhi, Andrea Vedaldi, Andrew Zisserman, and C. V. Jawahar. Cats and dogs. In *2012 IEEE Conference on Computer Vision and Pattern Recognition, Providence, RI, USA, June 16-21, 2012*, pages 3498–3505. IEEE Computer Society, 2012.

[40] Eleonora Poeta, Gabriele Ciravegna, Eliana Pastor, Tania Cerquitelli, and Elena Baralis. Concept-based explainable artificial intelligence: A survey. *ArXiv preprint*, abs/2312.12936, 2023.

[41] Alec Radford, Jong Wook Kim, Chris Hallacy, Aditya Ramesh, Gabriel Goh, Sandhini Agarwal, Girish Sastry, Amanda Askell, Pamela Mishkin, Jack Clark, Gretchen Krueger, and Ilya Sutskever. Learning transferable visual models from natural language supervision. In Marina Meila and Tong Zhang, editors, *Proceedings of the 38th International Conference on Machine Learning, ICML 2021, 18-24 July 2021, Virtual Event*, volume 139 of *Proceedings of Machine Learning Research*, pages 8748–8763. PMLR, 2021.

[42] Anna Rohrbach, Lisa Anne Hendricks, Kaylee Burns, Trevor Darrell, and Kate Saenko. Object hallucination in image captioning. In Ellen Riloff, David Chiang, Julia Hockenmaier, and Jun’ichi Tsujii, editors, *Proceedings of the 2018 Conference on Empirical Methods in Natural Language Processing*, pages 4035–4045, Brussels, Belgium, 2018. Association for Computational Linguistics.

[43] Christoph Schuhmann, Romain Beaumont, Richard Vencu, Cade Gordon, Ross Wightman, Mehdi Cherti, Theo Coombes, Aarush Katta, Clayton Mullis, Mitchell Wortsman, Patrick Schramowski, Srivatsa Kundurthy, Katherine Crowson, Ludwig Schmidt, Robert Kaczmarczyk, and Jenia Jitsev. LAION-5B: an open large-scale dataset for training next generation image-text models. In Sanmi Koyejo, S. Mohamed, A. Agarwal, Danielle Belgrave, K. Cho, and A. Oh, editors, *Advances in Neural Information Processing Systems 35: Annual Conference on Neural Information Processing Systems 2022, NeurIPS 2022, New Orleans, LA, USA, November 28 - December 9, 2022*, 2022.

[44] Sarah Schwettmann, Neil Chowdhury, Samuel Klein, David Bau, and Antonio Torralba. Multi-modal neurons in pretrained text-only transformers. In *IEEE/CVF International Conference on Computer Vision, ICCV 2023 - Workshops, Paris, France, October 2-6, 2023*, pages 2854–2859. IEEE, 2023.

[45] Piyush Sharma, Nan Ding, Sebastian Goodman, and Radu Soricut. Conceptual captions: A cleaned, hypernymed, image alt-text dataset for automatic image captioning. In Iryna Gurevych and Yusuke Miyao, editors, *Proceedings of the 56th Annual Meeting of the Association for Computational Linguistics (Volume 1: Long Papers)*, pages 2556–2565, Melbourne, Australia, 2018. Association for Computational Linguistics.

[46] Shufan Shen, Zhaobo Qi, Junshu Sun, Qingming Huang, Qi Tian, and Shuhui Wang. Enhancing pre-trained representation classifiability can boost its interpretability. In *The Thirteenth International Conference on Learning Representations, ICLR 2025, Singapore, April 24-28, 2025*. OpenReview.net, 2025.

[47] Shufan Shen, Junshu Sun, Xiangyang Ji, Qingming Huang, and Shuhui Wang. Expanding sparse tuning for low memory usage. In Amir Globersons, Lester Mackey, Danielle Belgrave, Angela Fan, Ulrich Paquet, Jakub M. Tomczak, and Cheng Zhang, editors, *Advances in Neural Information Processing Systems 38: Annual Conference on Neural Information Processing Systems 2024, NeurIPS 2024, Vancouver, BC, Canada, December 10 - 15, 2024*, 2024.

[48] Shufan Shen, Junshu Sun, Shuhui Wang, and Qingming Huang. Kernelized sparse fine-tuning with bi-level parameter competition for vision models. *arXiv preprint arXiv:2510.24037*, 2025.

[49] Dong Shu, Haiyan Zhao, Jingyu Hu, Weiru Liu, Ali Payani, Lu Cheng, and Mengnan Du. Large vision-language model alignment and misalignment: A survey through the lens of explainability. *ArXiv preprint*, abs/2501.01346, 2025.

[50] Mustafa Shukor and Matthieu Cord. Implicit multimodal alignment: On the generalization of frozen llms to multimodal inputs. *ArXiv preprint*, abs/2405.16700, 2024.

[51] Richard Socher, Alex Perelygin, Jean Wu, Jason Chuang, Christopher D. Manning, Andrew Ng, and Christopher Potts. Recursive deep models for semantic compositionality over a sentiment treebank. In David Yarowsky, Timothy Baldwin, Anna Korhonen, Karen Livescu, and Steven Bethard, editors, *Proceedings of the 2013 Conference on Empirical Methods in Natural Language Processing*, pages 1631–1642, Seattle, Washington, USA, 2013. Association for Computational Linguistics.

[52] Junshu Sun, Wanxing Chang, Chenxue Yang, Qingming Huang, and Shuhui Wang. Relieving the Over-Aggregating Effect in Graph Transformers, 2025.

[53] Junshu Sun, Shuhui Wang, Xinzhe Han, Zhe Xue, and Qingming Huang. All in a row: Compressed convolution networks for graphs. In *Proceedings of the 40th International Conference on Machine Learning*, volume 202 of *Proceedings of Machine Learning Research*, pages 33061–33076. PMLR, 23–29 Jul 2023.

[54] Junshu Sun, Chenxue Yang, Xiangyang Ji, Qingming Huang, and Shuhui Wang. Towards dynamic message passing on graphs. In *Advances in Neural Information Processing Systems*, volume 37, pages 80936–80964. Curran Associates, Inc., 2024.

[55] Gemini Team, Rohan Anil, Sebastian Borgeaud, Jean-Baptiste Alayrac, Jiahui Yu, Radu Soricut, Johan Schalkwyk, Andrew M Dai, Anja Hauth, Katie Millican, et al. Gemini: a family of highly capable multimodal models. *ArXiv preprint*, abs/2312.11805, 2023.

[56] Hugo Touvron, Louis Martin, Kevin Stone, Peter Albert, Amjad Almahairi, Yasmine Babaei, Nikolay Bashlykov, Soumya Batra, Prajjwal Bhargava, Shruti Bhosale, et al. Llama 2: Open foundation and fine-tuned chat models. *ArXiv preprint*, abs/2307.09288, 2023.

[57] Cheng-Hao Tu, Zheda Mai, and Wei-Lun Chao. Visual query tuning: Towards effective usage of intermediate representations for parameter and memory efficient transfer learning. In *IEEE/CVF Conference on Computer Vision and Pattern Recognition, CVPR 2023, Vancouver, BC, Canada, June 17-24, 2023*, pages 7725–7735. IEEE, 2023.

[58] Laurens Van der Maaten and Geoffrey Hinton. Visualizing data using t-sne. *Journal of machine learning research*, 9(11), 2008.

[59] Catherine Wah, Steve Branson, Peter Welinder, Pietro Perona, and Serge Belongie. The caltech-ucsd birds-200-2011 dataset. 2011.

[60] Peng Wang, Shuai Bai, Sinan Tan, Shijie Wang, Zhihao Fan, Jinze Bai, Keqin Chen, Xuejing Liu, Jialin Wang, Wenbin Ge, et al. Qwen2-vl: Enhancing vision-language model’s perception of the world at any resolution. *ArXiv preprint*, abs/2409.12191, 2024.

[61] Jianxiong Xiao, James Hays, Krista A. Ehinger, Aude Oliva, and Antonio Torralba. SUN database: Large-scale scene recognition from abbey to zoo. In *The Twenty-Third IEEE Conference on Computer Vision and Pattern Recognition, CVPR 2010, San Francisco, CA, USA, 13-18 June 2010*, pages 3485–3492. IEEE Computer Society, 2010.

[62] Xinyue Xu, Yi Qin, Lu Mi, Hao Wang, and Xiaomeng Li. Energy-based concept bottleneck models: Unifying prediction, concept intervention, and probabilistic interpretations. In *The Twelfth International Conference on Learning Representations, ICLR 2024, Vienna, Austria, May 7-11, 2024*. OpenReview.net, 2024.

[63] Mert Yüksekgönül, Maggie Wang, and James Zou. Post-hoc concept bottleneck models. In *The Eleventh International Conference on Learning Representations, ICLR 2023, Kigali, Rwanda, May 1-5, 2023*. OpenReview.net, 2023.

- [64] Mateo Espinosa Zarlenga, Pietro Barbiero, Gabriele Ciravegna, Giuseppe Marra, Francesco Giannini, Michelangelo Diligenti, Zohreh Shams, Frédéric Precioso, Stefano Melacci, Adrian Weller, Pietro Lió, and Mateja Jamnik. Concept embedding models: Beyond the accuracy-explainability trade-off. In Sanmi Koyejo, S. Mohamed, A. Agarwal, Danielle Belgrave, K. Cho, and A. Oh, editors, *Advances in Neural Information Processing Systems 35: Annual Conference on Neural Information Processing Systems 2022, NeurIPS 2022, New Orleans, LA, USA, November 28 - December 9, 2022*, 2022.
- [65] Siqi Zhang, Yanyuan Qiao, Qunbo Wang, Longteng Guo, Zhihua Wei, and Jing Liu. Flexvln: Flexible adaptation for diverse vision-and-language navigation tasks. *arXiv preprint arXiv:2503.13966*, 2025.
- [66] Siqi Zhang, Yanyuan Qiao, Qunbo Wang, Zike Yan, Qi Wu, Zhihua Wei, and Jing Liu. Cosmo: Combination of selective memorization for low-cost vision-and-language navigation. *arXiv preprint arXiv:2503.24065*, 2025.
- [67] Chenyang Zhao, Kun Wang, Xingyu Zeng, Rui Zhao, and Antoni B Chan. Gradient-based visual explanation for transformer-based clip. In *International Conference on Machine Learning*, pages 61072–61091. PMLR, 2024.

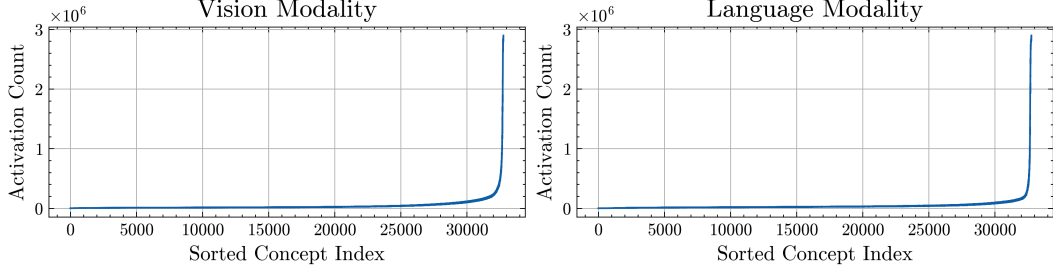


Figure A8: Activation count of each concept in VL-SAE constructed for LLaVA1.5 [34].

Table A6: The  $\alpha$  value of OpenCLIP with varying model sizes in zero-shot image classification tasks.

	Caltech101	Cifar10	Cifar100	Country211	DTD	Eurosat	Flowers	Food	GTSRB	MNIST	Pets	SST2	STL10	Sun397
ViT-B/32	0.6	0.6	0.3	0.1	0.1	0.2	0.1	0.5	0.4	1.0	0.1	0.3	0.1	0.2
ViT-B/16	0.6	0.5	0.3	0.1	0.1	0.1	0.1	0.5	0.5	1.0	0.1	0.2	0.1	0.2
ViT-L/14	0.6	0.4	0.3	0.3	0.1	0.3	0.2	0.1	0.2	1.0	0.1	0.1	0.9	0.1
ViT-H/14	0.4	0.8	0.6	0.1	0.3	0.7	0.1	0.9	0.5	1.0	0.1	0.5	0.2	0.1

## A More Implementation Details

### A.1 Details of the VL-SAE Construction and Evaluation

For the InfoNCE loss utilized in Section 3.2, given an image-text pair  $(\mathbf{x}_v^e, \mathbf{x}_l^e)$  and other  $N$  with intermediate representations  $\{(\mathbf{x}_{v,1}^e, \mathbf{x}_{l,1}^e), \dots, (\mathbf{x}_{v,N}^e, \mathbf{x}_{l,N}^e)\}$  which denote the  $(\mathbf{x}_v^{e-}, \mathbf{x}_l^{e-})$  in Equation 3, the InfoNCE loss can be represented by

$$\text{InfoNCE}(\mathbf{x}_v^e, \mathbf{x}_l^e, \mathbf{x}_v^{e-}, \mathbf{x}_l^{e-}) = -\log \left( \frac{\exp(\frac{\cos(\theta_{\mathbf{x}_v^e, \mathbf{x}_l^e})}{\tau})}{\sum_{i=1}^N \exp(\frac{\cos(\theta_{\mathbf{x}_v^e, \mathbf{x}_{l,i}^e})}{\tau})} \right) - \log \left( \frac{\exp(\frac{\cos(\theta_{\mathbf{x}_v^e, \mathbf{x}_l^{e-}})}{\tau})}{\sum_{i=1}^N \exp(\frac{\cos(\theta_{\mathbf{x}_{v,i}^e, \mathbf{x}_l^{e-}})}{\tau})} \right), \quad (\text{A12})$$

where  $\tau$  denotes the temperature hyperparameter, which is set to 0.07. The InfoNCE loss is computed for image-text pairs within the same batch and aggregated to train the auxiliary autoencoder.

For the construction of the VL-SAE and auxiliary autoencoder, all the modules except for the distance-based encoder are implemented with a linear layer. We set the hidden ratio to 8 in both CVLMs and LVLMs, indicating that the number of neurons in the hidden layer is 8 times the representation dimension. Unless otherwise specified, the number of activated neurons for each representation is set to 256 for all CVLMs and LVLMs. For the quantitative evaluation of the concept set, we randomly select several concepts from the autoencoder to compute their intra-similarity and inter-similarity. We calculate these metrics through five random trials, and the average value is adopted to be presented in Figure 3. The impact of the number of concepts used for evaluation is shown in Table A7. The metrics showed no significant differences when more than 100 concepts are used. Since the evaluation needs to be repeated multiple times, we select 100 concepts in each iteration for efficient evaluation.

For the evaluation metrics in Figure 3, for the  $i$ -th neuron, we first obtain its maximally activating images and texts. Then, these images and texts are transformed into representations with a pre-trained OpenCLIP-ViT-H/14 [43]. The averaged image and text representations  $\mathbf{x}_v^i, \mathbf{x}_l^i$  are utilized to compute the Inter-Similarity and Inter-Similarity metrics. The Inter-Similarity is computed as the average cosine similarity between the image and text representations within the same neuron.

$$\text{Sim}_{\text{intra}} = \frac{1}{h} \sum_{i=1}^h \cos(\theta_{\mathbf{x}_v^i, \mathbf{x}_l^i}). \quad (\text{A13})$$

Table A7: Impact of the number of concepts on the evaluation metrics based on OpenCLIP-ViT-B-16.

Concept Num.	100	200	300	400	500
Intra Similarity (SAE-S)	0.2200	0.2257	0.2281	0.2245	0.2247
Intra Similarity (VL-SAE)	<b>0.2445</b>	<b>0.2508</b>	<b>0.2489</b>	<b>0.2476</b>	<b>0.2469</b>
Inter Similarity (SAE-S)	0.1347	0.1293	0.1300	0.1306	0.1308
Inter Similarity (VL-SAE)	<b>0.1230</b>	<b>0.1214</b>	<b>0.1182</b>	<b>0.1181</b>	<b>0.1195</b>

Table A8: Number of concepts within different SAEs.

Method	Hidden Neuron	Dead Neuron	Concept Num.
SAE-D	32768 (4096×8)	54	32714
SAE-S	32768 (4096×8)	46	32722
VL-SAE	32768 (4096×8)	15	32753

For the Inter-Similarity, it is computed as the average cosine similarity between the image and text representations within the different neurons.

$$Sim_{inter} = \frac{1}{h(h-1)} \sum_{i=1}^h \sum_{j \neq i}^h \cos(\theta_{\mathbf{x}_v^i, \mathbf{x}_v^j}). \quad (A14)$$

For the resource requirements, the VL-SAE models for different VLMs [43, 34, 1] are all trained using a single NVIDIA GeForce RTX 4090 GPU. For CVLM [43], full-precision training is employed to ensure optimal performance and stability. For LVLM [34, 1], half-precision (FP16) training is utilized to effectively reduce resource requirements while maintaining model efficiency.

## A.2 Number of Concepts in VL-SAE

In Table A8, we provide the number of concepts in different SAE architectures based on LLaVA 1.5 with 4096 feature dimensions. The number of concepts is upper bounded by the number of hidden neurons in SAEs. Moreover, the number of concepts is influenced by the training process and SAE architectures. This stems from the inevitable existence of dead neurons in SAEs [15], which are never activated. The results show that VL-SAE learns more concepts compared to existing methods.

## A.3 Details of Interpreting Representations with VL-SAE.

We observe that a subset of concepts in VL-SAE are activated at high frequencies, as Figure A8 shown, *i.e.*, almost all samples activate these concepts. This frequent activation makes it challenging for these concepts to be associated with specific semantics, as shown in Tale A9. Consequently, in the interpretation process, we divide the target representation’s neuron activation by the average activation value of each neuron, thereby mitigating the impact of these high-frequency concepts on the interpretation.

Table A9: The concepts of VL-SAE relevant to a kitchen image with and without re-weighting. All concepts are shown in text form. The concept corresponding to the high-frequency neuron is denoted by (\*), which exhibits irrelevant semantics with the input kitchen image.

Before re-weighting	After re-weighting
toast popping out of a toaster	toast popping out of a toaster
hard rock artist performs (*)	burning on a gas stove in the kitchen
burning on a gas stove in the kitchen	cans in a refrigerator in a restaurant
cans in a refrigerator in a restaurant	this is a gas stove with electric ovens
this is a gas stove with electric ovens	gas fueled rings on a domestic cooker

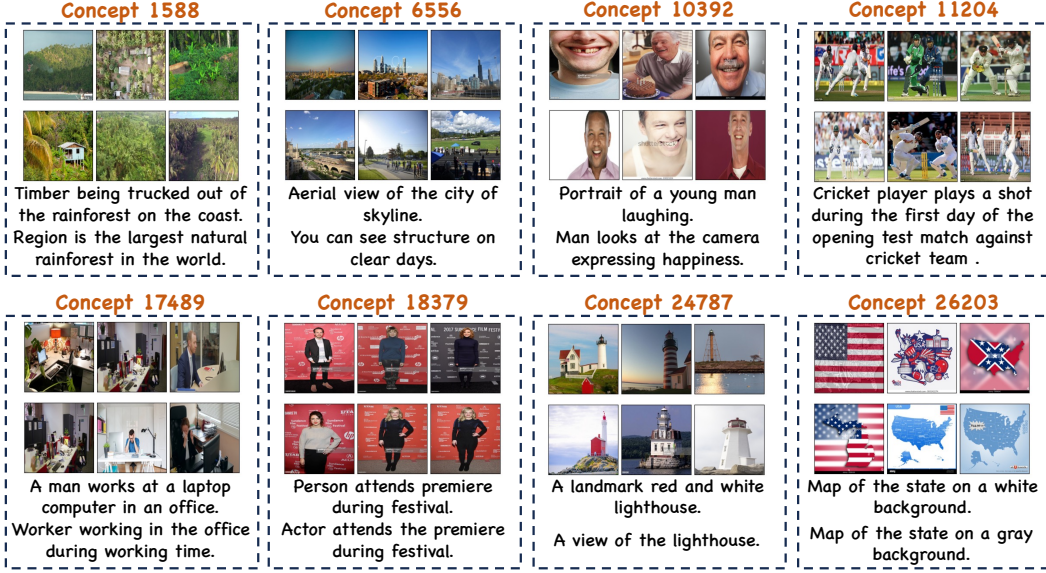


Figure A9: More concepts learned by VL-SAE. We provide the maximally activating images and texts for several concepts of VL-SAE trained for LLaVA1.5.

#### A.4 Details of the Zero-shot Image Classification Task

Considering the varying degrees of alignment between the concept set of VL-SAE and the target categories of the downstream task, we experiment with multiple values of  $\alpha \in \{0.1, 0.2, 0.3, 0.4, 0.5, 0.6, 0.7, 0.8, 0.9\}$  and select the one that performs best. The selected values are presented in Table A6. We observed that models of varying sizes tended to select different  $\alpha$  values, whereas for certain datasets like MNIST and Pets, the optimal alpha values remained consistent across different models. Moreover, we observe that the optimal alpha values for some datasets, such as CIFAR-10 and Caltech101, are significantly higher than those for other datasets. This discrepancy stems from the strong correlation between their target categories and the dataset utilized to train the VL-SAE model.

#### A.5 Details of the Hallucination Elimination Task

With the modified representation  $\hat{\mathbf{x}}_l$  in Equation 11, we adopt the contrastive decoding strategy [26] to mitigate the hallucination in LLMs. Specifically, with the representations of vision and language tokens  $\mathbf{x}_{vt} \in \mathbb{R}^{N_v \times d}$ ,  $\mathbf{x}_{lt} \in \mathbb{R}^{N_l \times d}$ , the model generates two distinct output distributions: (i) one conditioned on the original representations; and (ii) the other conditioned on the original vision representations and the language representations with their mean value across the token dimension replaced by  $\hat{\mathbf{x}}_l$ .

$$\hat{\mathbf{x}}_{lt}[i] = \mathbf{x}_{lt}[i] - \mathbf{x}_l + \hat{\mathbf{x}}_l, \quad (\text{A15})$$

where  $\mathbf{x}_{lt}[i] \in \mathbb{R}^d$  denotes the representation of the  $i$ -th text token,  $\mathbf{x}_l \in \mathbb{R}^d$  denotes the language representations averaged across the token dimension. Then, a new contrastive probability distribution is computed by exploiting the differences between the two initially obtained distributions. The new contrastive distribution is formulated as

$$p_{cd}(y | \mathbf{x}_{vt}, \mathbf{x}_{lt}, \hat{\mathbf{x}}_{lt}) = \text{softmax}[(1 - \alpha_{cd}) \text{logit}_\theta(y | \mathbf{x}_{vt}, \mathbf{x}_{lt}) + \alpha_{cd} \text{logit}_\theta(y | \mathbf{x}_{vt}, \hat{\mathbf{x}}_{lt})]. \quad (\text{A16})$$

Larger  $\alpha_{cd}$  values indicate a stronger amplification of differences between the two distributions. Moreover, we also utilize the adaptive plausibility constraints [29] that conduct contrastive decoding contingent upon the confidence level  $\beta_{cd}$  associated with the output distribution with original representations. In practice, we set  $\alpha_{cd}$  and  $\beta_{cd}$  to 0.6 and 0.8, respectively. Additionally, the values of  $\alpha$  and  $\beta$  in Equation 11 are determined to be 0.7 and 0.9, respectively.

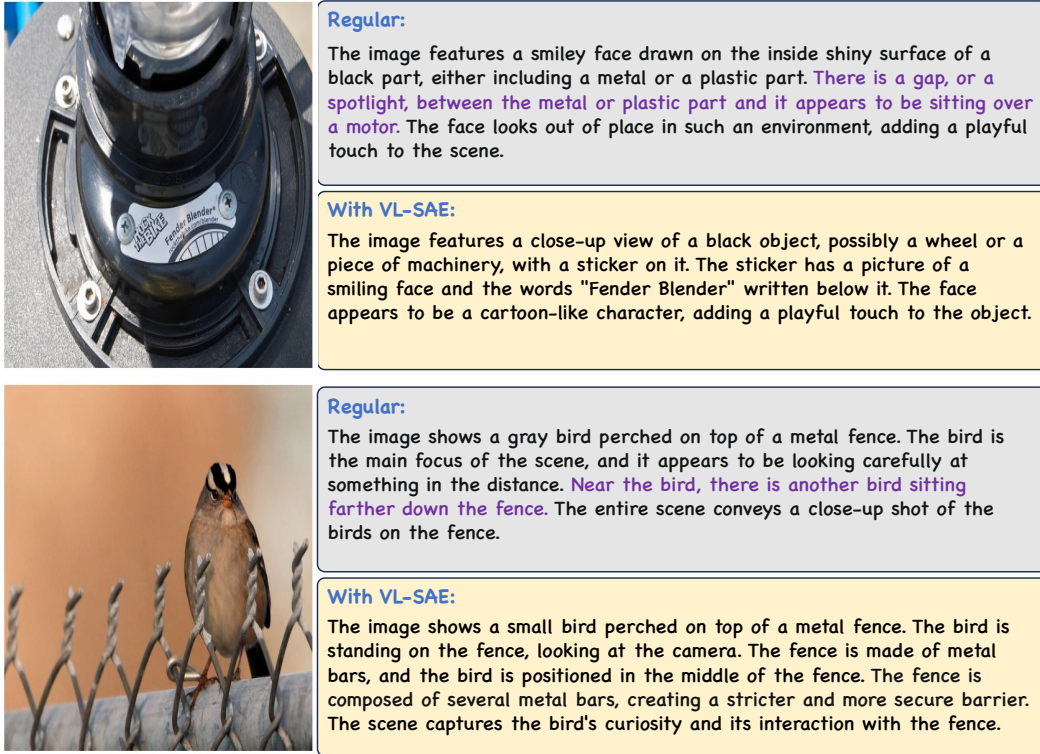


Figure A10: Illustration of generated captions by different decoding methods with LLaVA 1.5 as the backbone model. Hallucinated content is highlighted in purple.

Table A10: Human evaluation of concepts learned by different SAEs.

Method	OpenCLIP-ViT/H	LLaVA 1.5
SAE-D	0.6	0.1
SAE-S	33.5	35.8
VL-SAE	65.9	64.1

## B More Experimental Results

### B.1 Human Evaluation

We randomly select 100 concepts from SAE-D, SAE-S, and VL-SAE, respectively, and invite 10 participants to evaluate these concepts. For each iteration, participants are required to evaluate the quality of three given concepts and select the one with the highest quality. The method corresponding to the selected concept is awarded one point. The concept quality of these methods is measured by the average score assigned by all participants. As Table A10 shows, concepts learned by VL-SAE possess higher quality than those learned by other methods. This comparison further highlights the effectiveness of our proposed VL-SAE.

### B.2 More Results for Hallucination Elimination

Beyond the “Yes-or-No” discriminative evaluations on the POPE datasets, we evaluate the VL-SAE on open-ended caption generation using the CHAIR benchmark [42]. We randomly select 500 samples from CHAIR for evaluation and calculate the average of the results obtained from five independent trials. The results in Table A11 show the superior performance of VL-SAE over the compared methods. Specifically, VL-SAE reduces object hallucinations in generated captions, as evidenced by lower  $\text{CHAIR}_S$  and  $\text{CHAIR}_I$  scores. In addition, VL-SAE enhances the detail of the generated captions, as indicated by higher Recall scores.

Table A11: Results on the subset of CHAIR.

Model	Decoding	CHAIR <sub>S</sub> (↓)	CHAIR <sub>I</sub> (↓)	Recall (↑)	Avg. Len
LLaVA1.5	Regular	53.4	17.6	72.3	103.2
	VCD	55.0	16.3	76.0	102.5
	VL-SAE	<b>47.8</b>	<b>13.3</b>	<b>76.3</b>	100.7
Qwen-VL	Regular	44.6	16.1	60.7	97.2
	VCD	42.6	13.9	60.0	94.1
	VL-SAE	<b>39.6</b>	<b>10.7</b>	<b>63.3</b>	94.0

Table A12: Training cost of VL-SAE based on representations of OpenCLIP.

Base Model	ViT-B/16	ViT-L/14	ViT-H/14
FLOPs	0.03G	0.06G	0.10G
Training Time	132s	228s	446s

### B.3 Resource Requirements of VL-SAE

**Training Costs.** Table A12 presents the training cost of VL-SAE. First, as the model size increases, the dimensionality of its learned representations grows, leading to higher computational demands for training VL-SAE. Second, despite this scaling trend, the overall training cost of VL-SAE remains remarkably low. For instance, when compared to LoRA [20], a widely adopted method known for its computational efficiency, training VL-SAE on OpenCLIP-ViT-B/16 representations incurs significantly fewer FLOPs (0.03G v.s. 1.91G). This minimal computational overhead stems from the small parameter volume in VL-SAE, which is approximately equivalent to that of two linear layers.

**Inference Cost.** Table A13 shows the parameters and computation cost of VL-SAE. For inference speed, we present the influences of VL-SAE in Table A14. The results indicate that VL-SAE has a negligible impact. This is because VL-SAE comprises only two linear layers with significantly smaller parameters than pre-trained VLMs.

### B.4 Additional Ablation Studies

**Selection of Hyperparameter  $\alpha_c$ .** We first provide accuracy comparisons under three settings: baseline ( $\alpha_c = 0$ ), task-agnostic ( $\alpha_c = 0.1$ ), and task-specific ( $\alpha_c$  determined by tasks). The results are shown in Table A15. First, the task-agnostic scheme performs better than the baseline (72.4% v.s. 72.2% on ViT-L, and 77.2% v.s. 76.9% on ViT-H). This indicates that  $\alpha$  does not need to be task-specific for performance improvement and can generalize across tasks. However, these tasks originate from different domains and exhibit distinct preferences for hyperparameters [31], as evidenced by the best performance of the task-specific scheme. If the objective is to achieve optimal performance, the  $\alpha$  values of each task should be determined individually. To determine the  $\alpha$  value of each task, we conduct experiments with multiple values  $\alpha \in [0, 1]$  at intervals of 0.1 and select the one that performs the best. Note that the cost of conducting multiple experiments is very low. For instance, when using the Food-101 dataset, each experiment on a single NVIDIA 4090 GPU takes only approximately 90 seconds.

**Selection of Hyperparameter  $\alpha_l$ .** For the hyperparameter  $\alpha_l$  in Equation 11, We conduct experiments by selecting values at intervals of 0.1 within the range of [0.5 – 0.9], and the one with the best performance is selected. We report the performance under different values in Table A16. The highest performance across different settings is achieved at  $\alpha_l = 0.7$ .

Table A13: Additional parameter and computation cost of VL-SAE.

Model	Total Param.	VL-SAE Param.	Total FLOPs	VL-SAE FLOPs
LLaVA-1.5	7529M	467M	14.03G	0.875G
OpenCLIP-ViT-H	1011M	25M	3.15G	0.034G

Table A14: Throughput (sample/s) of the original models and those equipped with VL-SAE.

Method	OpenCLIP-ViT-B	OpenCLIP-ViT-L	OpenCLIP-ViT-H	LLaVA 1.5
Original	935.32	213.62	99.45	11.34
+VL-SAE	935.13	213.42	99.29	10.69

Table A15: Ablation of hyperparameter  $\alpha_c$  in Equation 10.

Method	OpenCLIP-ViT-L	OpenCLIP-ViT-H
baseline ( $\alpha_c = 0$ )	72.2	76.9
task-agnostic ( $\alpha_c = 0.1$ )	72.4	77.2
task-specific ( $\alpha_c$ determined by tasks)	<b>72.9</b>	<b>77.8</b>

**CC3M training.** In the training process of VL-SAE, the CC3M dataset is employed to integrate VL-SAE as a general plug-in for VLMs, rather than to augment the intrinsic capabilities of these VLMs. In our training strategies, the VLM parameters remain frozen without any adjustments. To further evaluate the impact of CC3M dataset, we provide comparisons between the base model (CLIP-ViT-B/16), the base model fine-tuned by CC3M, and the base model equipped with VL-SAE in Table A17. The results show that fine-tuning does not lead to improved performance on downstream tasks. This is because CC3M serves as a subset of the VLM pre-training dataset. It does not provide the base model with any additional task-relevant information. The superior performance of VL-SAE compared to the fine-tuning model indicates that the improvement stems from the mapping from representations to concepts, rather than the incorporation of CC3M.

## B.5 Additional Visualizations

### B.5.1 Concepts Learned by VL-SAE

We provide more visualization of the concepts learned by VL-SAE in Figure A9. These results highlight the superior capability of VL-SAE in acquiring a vision-language concept set with rich semantics, such as natural landscapes, urban environments, human expressions, and maps.

### B.5.2 Cases for Hallucination Elimination

We present qualitative examples of different decoding methods in Figure A10. Regular decoding [34] often produces object hallucinations, especially in the latter part of the outputs. In contrast, utilizing VL-SAE effectively mitigates the object hallucinations by enhancing the vision-language alignment at the concept level during the decoding process.

### B.5.3 Visualization of the Representations and Learnable Weights

Figure A11 illustrates the t-SNE [58] visualization for the vision-language representations of VLMs and the learnable weights in the encoder of the VL-SAE. We observe that the majority of learnable weights are positioned midway between vision and language representations, rather than being skewed toward either modality. This position enables the corresponding neurons to exhibit consistent activation values across different modalities, which helps map the vision-language representations into a unified concept set.

Table A16: Ablation studies on the hyperparameter  $\alpha_l$  of Equation 11. All experiments are conducted on POPE benchmark with LLaVA 1.5.

Setting	0.5	0.6	0.7	0.8	0.9
Random	85.29	85.32	<b>85.50</b>	85.41	85.31
Popular	84.09	84.15	<b>84.37</b>	84.23	84.12
Adversarial	81.92	82.10	<b>82.29</b>	81.95	81.93

Table A17: Ablation studies on the impact of the CC3M dataset.

Method	Base Model	Base Model+Fine-tuning	Base Model+VL-SAE
Mean Accuracy	69.8	69.7	70.4

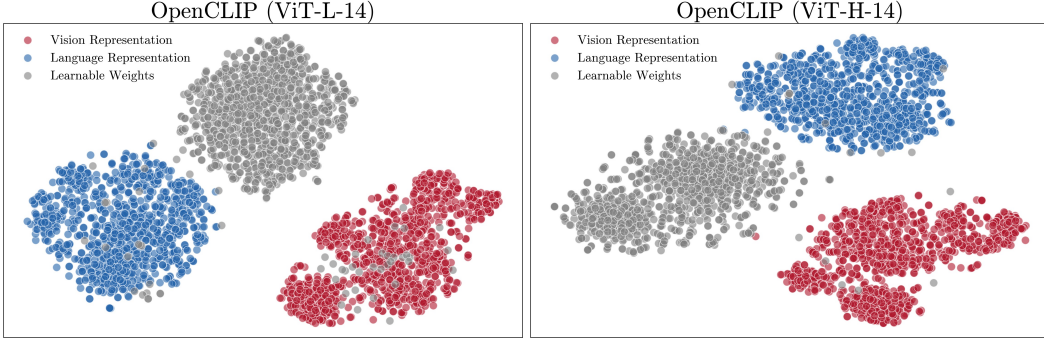


Figure A11: Visualizations of the vision-language representations in the VLMs and the learnable weights in the VL-SAE encoder. Experiments are conducted with t-SNE [58] for dimension reduction.

## C Discussion

### C.1 Criterion of Representation Selection in LVLMs

We extract the representations from the outputs of the 29-th layer in LLaVA 1.5 and the 26-th layer in Qwen-VL. These layers are chosen because the representations in the top layers tend to be more interpretable in terms of concepts [23]. Furthermore, at these layers, both vision and language representations preserve their respective information effectively. As shown in Figure A12, starting from the 27-th layer of Qwen-VL, the distributions of the two types of representations begin to converge, leading to a potential loss of distinct visual information. This convergence hinders the process of leveraging vision representations to constrain language representations for reducing hallucinations.

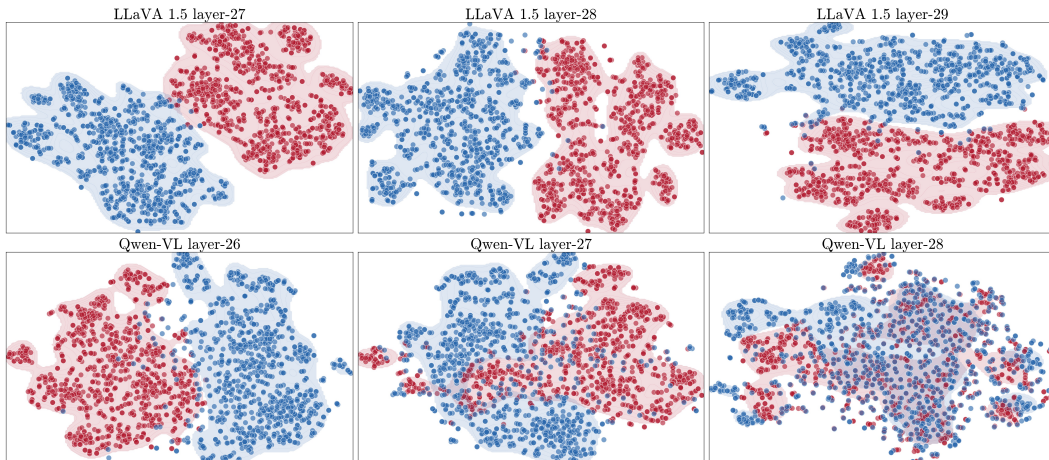


Figure A12: Visualizations of the vision-language representations in different layers of VLMs. Experiments are conducted with t-SNE [58] for dimension reduction.

## C.2 Metrics for Evaluating the Concept Set

For the quantitative evaluation of concept collections, we utilized CLIP similarity for automated assessment in Figure 3 and Table 3. However, the numerical differences in CLIP similarity might not entirely capture the improvements in concept quality achieved by VL-SAE relative to other methods. This is because the numerical gap in CLIP similarity between semantically similar and dissimilar image-text pairs can sometimes be minimal. Therefore, it is important to establish a more comprehensive evaluation mechanism for SAEs based on multi-modal representations in the future.

## C.3 Discussions with attribution-based methods

We discuss and compare VL-SAE, a concept-based approach, with attribution-based methods [67, 4] for VLMs, enabling users to select the most appropriate method based on specific application scenarios. Attribution-based methods generate a heatmap for each input sample to indicate the importance of individual components of the input data (*e.g.*, image pixels), whereas VL-SAE constructs a concept set across varying samples to interpret the semantics of their hidden representations.

Based on their paradigms, we compare them in the perspective of *intuitiveness*, *expressivity* and *ability to improve model performance*. (*i*) Intuitiveness. Compared with VL-SAE, attribution-based methods offer a more intuitive interpretation, as they visualize attribution scores directly on input images. (*ii*) Expressivity. Compared with attribution-based methods, VL-SAE exhibits stronger expressivity as it reveals how the model understands the semantics of input data with concepts, rather than simply providing numerical information to identify the important image regions. (*iii*) Ability to improve model performance. In contrast to attribution-based methods that only serve as an observer for model prediction, VL-SAE can act as an intervener to improve model performance by modifying hidden representations during inference.

## C.4 Limitation Discussion

Despite successfully correlating the semantics of vision-language representations with a unified concept set, the VL-SAE encounters the same challenges as the SAE architectures for other models (*e.g.*, LLMs [56] and vision models [12, 5]), such as dead neurons [15], limited relational modeling, and the impact of high-frequency neurons on interpretations as shown in Figure A8. Additionally, the strategy of enhancing the alignment mechanism with VL-SAE is simple and fails to fully unlock the potential of the unified concept set. To address these limitations, we anticipate future work to design SAEs that encourage the neurons to be uniformly activated, incorporate relational modeling [53, 54, 52] among concepts, and enable more effective integration into the prediction processes of VLMs.

## NeurIPS Paper Checklist

### 1. Claims

Question: Do the main claims made in the abstract and introduction accurately reflect the paper's contributions and scope?

Answer: [\[Yes\]](#)

Justification: The main claims made in the abstract and introduction accurately reflect the paper's contributions and scope.

Guidelines:

- The answer NA means that the abstract and introduction do not include the claims made in the paper.
- The abstract and/or introduction should clearly state the claims made, including the contributions made in the paper and important assumptions and limitations. A No or NA answer to this question will not be perceived well by the reviewers.
- The claims made should match theoretical and experimental results, and reflect how much the results can be expected to generalize to other settings.
- It is fine to include aspirational goals as motivation as long as it is clear that these goals are not attained by the paper.

### 2. Limitations

Question: Does the paper discuss the limitations of the work performed by the authors?

Answer: [\[Yes\]](#)

Justification: We discuss the limitation in Appendix [C.4](#)

Guidelines:

- The answer NA means that the paper has no limitation while the answer No means that the paper has limitations, but those are not discussed in the paper.
- The authors are encouraged to create a separate "Limitations" section in their paper.
- The paper should point out any strong assumptions and how robust the results are to violations of these assumptions (e.g., independence assumptions, noiseless settings, model well-specification, asymptotic approximations only holding locally). The authors should reflect on how these assumptions might be violated in practice and what the implications would be.
- The authors should reflect on the scope of the claims made, e.g., if the approach was only tested on a few datasets or with a few runs. In general, empirical results often depend on implicit assumptions, which should be articulated.
- The authors should reflect on the factors that influence the performance of the approach. For example, a facial recognition algorithm may perform poorly when image resolution is low or images are taken in low lighting. Or a speech-to-text system might not be used reliably to provide closed captions for online lectures because it fails to handle technical jargon.
- The authors should discuss the computational efficiency of the proposed algorithms and how they scale with dataset size.
- If applicable, the authors should discuss possible limitations of their approach to address problems of privacy and fairness.
- While the authors might fear that complete honesty about limitations might be used by reviewers as grounds for rejection, a worse outcome might be that reviewers discover limitations that aren't acknowledged in the paper. The authors should use their best judgment and recognize that individual actions in favor of transparency play an important role in developing norms that preserve the integrity of the community. Reviewers will be specifically instructed to not penalize honesty concerning limitations.

### 3. Theory assumptions and proofs

Question: For each theoretical result, does the paper provide the full set of assumptions and a complete (and correct) proof?

Answer: [\[NA\]](#)

Justification: This paper does not include theoretical results.

Guidelines:

- The answer NA means that the paper does not include theoretical results.
- All the theorems, formulas, and proofs in the paper should be numbered and cross-referenced.
- All assumptions should be clearly stated or referenced in the statement of any theorems.
- The proofs can either appear in the main paper or the supplemental material, but if they appear in the supplemental material, the authors are encouraged to provide a short proof sketch to provide intuition.
- Inversely, any informal proof provided in the core of the paper should be complemented by formal proofs provided in appendix or supplemental material.
- Theorems and Lemmas that the proof relies upon should be properly referenced.

#### 4. Experimental result reproducibility

Question: Does the paper fully disclose all the information needed to reproduce the main experimental results of the paper to the extent that it affects the main claims and/or conclusions of the paper (regardless of whether the code and data are provided or not)?

Answer: **[Yes]**

Justification: Please refer to Section 4.1, Appendix A and the codes in the supplementary.

Guidelines:

- The answer NA means that the paper does not include experiments.
- If the paper includes experiments, a No answer to this question will not be perceived well by the reviewers: Making the paper reproducible is important, regardless of whether the code and data are provided or not.
- If the contribution is a dataset and/or model, the authors should describe the steps taken to make their results reproducible or verifiable.
- Depending on the contribution, reproducibility can be accomplished in various ways. For example, if the contribution is a novel architecture, describing the architecture fully might suffice, or if the contribution is a specific model and empirical evaluation, it may be necessary to either make it possible for others to replicate the model with the same dataset, or provide access to the model. In general, releasing code and data is often one good way to accomplish this, but reproducibility can also be provided via detailed instructions for how to replicate the results, access to a hosted model (e.g., in the case of a large language model), releasing of a model checkpoint, or other means that are appropriate to the research performed.
- While NeurIPS does not require releasing code, the conference does require all submissions to provide some reasonable avenue for reproducibility, which may depend on the nature of the contribution. For example
  - (a) If the contribution is primarily a new algorithm, the paper should make it clear how to reproduce that algorithm.
  - (b) If the contribution is primarily a new model architecture, the paper should describe the architecture clearly and fully.
  - (c) If the contribution is a new model (e.g., a large language model), then there should either be a way to access this model for reproducing the results or a way to reproduce the model (e.g., with an open-source dataset or instructions for how to construct the dataset).
  - (d) We recognize that reproducibility may be tricky in some cases, in which case authors are welcome to describe the particular way they provide for reproducibility. In the case of closed-source models, it may be that access to the model is limited in some way (e.g., to registered users), but it should be possible for other researchers to have some path to reproducing or verifying the results.

#### 5. Open access to data and code

Question: Does the paper provide open access to the data and code, with sufficient instructions to faithfully reproduce the main experimental results, as described in supplemental material?

Answer: [\[Yes\]](#)

Justification: Please refer to the codes in the supplementary.

Guidelines:

- The answer NA means that paper does not include experiments requiring code.
- Please see the NeurIPS code and data submission guidelines (<https://nips.cc/public/guides/CodeSubmissionPolicy>) for more details.
- While we encourage the release of code and data, we understand that this might not be possible, so “No” is an acceptable answer. Papers cannot be rejected simply for not including code, unless this is central to the contribution (e.g., for a new open-source benchmark).
- The instructions should contain the exact command and environment needed to run to reproduce the results. See the NeurIPS code and data submission guidelines (<https://nips.cc/public/guides/CodeSubmissionPolicy>) for more details.
- The authors should provide instructions on data access and preparation, including how to access the raw data, preprocessed data, intermediate data, and generated data, etc.
- The authors should provide scripts to reproduce all experimental results for the new proposed method and baselines. If only a subset of experiments are reproducible, they should state which ones are omitted from the script and why.
- At submission time, to preserve anonymity, the authors should release anonymized versions (if applicable).
- Providing as much information as possible in supplemental material (appended to the paper) is recommended, but including URLs to data and code is permitted.

## 6. Experimental setting/details

Question: Does the paper specify all the training and test details (e.g., data splits, hyper-parameters, how they were chosen, type of optimizer, etc.) necessary to understand the results?

Answer: [\[Yes\]](#)

Justification: Please refer to Section 4.1.

Guidelines:

- The answer NA means that the paper does not include experiments.
- The experimental setting should be presented in the core of the paper to a level of detail that is necessary to appreciate the results and make sense of them.
- The full details can be provided either with the code, in appendix, or as supplemental material.

## 7. Experiment statistical significance

Question: Does the paper report error bars suitably and correctly defined or other appropriate information about the statistical significance of the experiments?

Answer: [\[No\]](#)

Justification: This paper does not report error bars following the practice of previous studies [8, 32].

Guidelines:

- The answer NA means that the paper does not include experiments.
- The authors should answer “Yes” if the results are accompanied by error bars, confidence intervals, or statistical significance tests, at least for the experiments that support the main claims of the paper.
- The factors of variability that the error bars are capturing should be clearly stated (for example, train/test split, initialization, random drawing of some parameter, or overall run with given experimental conditions).
- The method for calculating the error bars should be explained (closed form formula, call to a library function, bootstrap, etc.)
- The assumptions made should be given (e.g., Normally distributed errors).

- It should be clear whether the error bar is the standard deviation or the standard error of the mean.
- It is OK to report 1-sigma error bars, but one should state it. The authors should preferably report a 2-sigma error bar than state that they have a 96% CI, if the hypothesis of Normality of errors is not verified.
- For asymmetric distributions, the authors should be careful not to show in tables or figures symmetric error bars that would yield results that are out of range (e.g. negative error rates).
- If error bars are reported in tables or plots, The authors should explain in the text how they were calculated and reference the corresponding figures or tables in the text.

## 8. Experiments compute resources

Question: For each experiment, does the paper provide sufficient information on the computer resources (type of compute workers, memory, time of execution) needed to reproduce the experiments?

Answer: [\[Yes\]](#)

Justification: Please refer to Appendix [A](#).

Guidelines:

- The answer NA means that the paper does not include experiments.
- The paper should indicate the type of compute workers CPU or GPU, internal cluster, or cloud provider, including relevant memory and storage.
- The paper should provide the amount of compute required for each of the individual experimental runs as well as estimate the total compute.
- The paper should disclose whether the full research project required more compute than the experiments reported in the paper (e.g., preliminary or failed experiments that didn't make it into the paper).

## 9. Code of ethics

Question: Does the research conducted in the paper conform, in every respect, with the NeurIPS Code of Ethics <https://neurips.cc/public/EthicsGuidelines>?

Answer: [\[Yes\]](#)

Justification: This paper conforms with the NeurIPS Code of Ethics.

Guidelines:

- The answer NA means that the authors have not reviewed the NeurIPS Code of Ethics.
- If the authors answer No, they should explain the special circumstances that require a deviation from the Code of Ethics.
- The authors should make sure to preserve anonymity (e.g., if there is a special consideration due to laws or regulations in their jurisdiction).

## 10. Broader impacts

Question: Does the paper discuss both potential positive societal impacts and negative societal impacts of the work performed?

Answer: [\[NA\]](#)

Justification: There is no societal impact of the work performed. Because it just focuses on the internal mechanism of pre-trained models.

Guidelines:

- The answer NA means that there is no societal impact of the work performed.
- If the authors answer NA or No, they should explain why their work has no societal impact or why the paper does not address societal impact.
- Examples of negative societal impacts include potential malicious or unintended uses (e.g., disinformation, generating fake profiles, surveillance), fairness considerations (e.g., deployment of technologies that could make decisions that unfairly impact specific groups), privacy considerations, and security considerations.

- The conference expects that many papers will be foundational research and not tied to particular applications, let alone deployments. However, if there is a direct path to any negative applications, the authors should point it out. For example, it is legitimate to point out that an improvement in the quality of generative models could be used to generate deepfakes for disinformation. On the other hand, it is not needed to point out that a generic algorithm for optimizing neural networks could enable people to train models that generate Deepfakes faster.
- The authors should consider possible harms that could arise when the technology is being used as intended and functioning correctly, harms that could arise when the technology is being used as intended but gives incorrect results, and harms following from (intentional or unintentional) misuse of the technology.
- If there are negative societal impacts, the authors could also discuss possible mitigation strategies (e.g., gated release of models, providing defenses in addition to attacks, mechanisms for monitoring misuse, mechanisms to monitor how a system learns from feedback over time, improving the efficiency and accessibility of ML).

## 11. Safeguards

Question: Does the paper describe safeguards that have been put in place for responsible release of data or models that have a high risk for misuse (e.g., pretrained language models, image generators, or scraped datasets)?

Answer: [NA]

Justification: This paper poses no such risks.

Guidelines:

- The answer NA means that the paper poses no such risks.
- Released models that have a high risk for misuse or dual-use should be released with necessary safeguards to allow for controlled use of the model, for example by requiring that users adhere to usage guidelines or restrictions to access the model or implementing safety filters.
- Datasets that have been scraped from the Internet could pose safety risks. The authors should describe how they avoided releasing unsafe images.
- We recognize that providing effective safeguards is challenging, and many papers do not require this, but we encourage authors to take this into account and make a best faith effort.

## 12. Licenses for existing assets

Question: Are the creators or original owners of assets (e.g., code, data, models), used in the paper, properly credited and are the license and terms of use explicitly mentioned and properly respected?

Answer: [Yes]

Justification: Please refer to Section 4.1 and Appendix A.

Guidelines:

- The answer NA means that the paper does not use existing assets.
- The authors should cite the original paper that produced the code package or dataset.
- The authors should state which version of the asset is used and, if possible, include a URL.
- The name of the license (e.g., CC-BY 4.0) should be included for each asset.
- For scraped data from a particular source (e.g., website), the copyright and terms of service of that source should be provided.
- If assets are released, the license, copyright information, and terms of use in the package should be provided. For popular datasets, [paperswithcode.com/datasets](https://paperswithcode.com/datasets) has curated licenses for some datasets. Their licensing guide can help determine the license of a dataset.
- For existing datasets that are re-packaged, both the original license and the license of the derived asset (if it has changed) should be provided.

- If this information is not available online, the authors are encouraged to reach out to the asset's creators.

### 13. New assets

Question: Are new assets introduced in the paper well documented and is the documentation provided alongside the assets?

Answer: [Yes]

Justification: Please refer to the codes in the supplementary.

Guidelines:

- The answer NA means that the paper does not release new assets.
- Researchers should communicate the details of the dataset/code/model as part of their submissions via structured templates. This includes details about training, license, limitations, etc.
- The paper should discuss whether and how consent was obtained from people whose asset is used.
- At submission time, remember to anonymize your assets (if applicable). You can either create an anonymized URL or include an anonymized zip file.

### 14. Crowdsourcing and research with human subjects

Question: For crowdsourcing experiments and research with human subjects, does the paper include the full text of instructions given to participants and screenshots, if applicable, as well as details about compensation (if any)?

Answer: [NA]

Justification: The paper does not involve crowdsourcing nor research with human subjects.

Guidelines:

- The answer NA means that the paper does not involve crowdsourcing nor research with human subjects.
- Including this information in the supplemental material is fine, but if the main contribution of the paper involves human subjects, then as much detail as possible should be included in the main paper.
- According to the NeurIPS Code of Ethics, workers involved in data collection, curation, or other labor should be paid at least the minimum wage in the country of the data collector.

### 15. Institutional review board (IRB) approvals or equivalent for research with human subjects

Question: Does the paper describe potential risks incurred by study participants, whether such risks were disclosed to the subjects, and whether Institutional Review Board (IRB) approvals (or an equivalent approval/review based on the requirements of your country or institution) were obtained?

Answer: [NA]

Justification: This paper does not involve crowdsourcing nor research with human subjects.

Guidelines:

- The answer NA means that the paper does not involve crowdsourcing nor research with human subjects.
- Depending on the country in which research is conducted, IRB approval (or equivalent) may be required for any human subjects research. If you obtained IRB approval, you should clearly state this in the paper.
- We recognize that the procedures for this may vary significantly between institutions and locations, and we expect authors to adhere to the NeurIPS Code of Ethics and the guidelines for their institution.
- For initial submissions, do not include any information that would break anonymity (if applicable), such as the institution conducting the review.

### 16. Declaration of LLM usage

Question: Does the paper describe the usage of LLMs if it is an important, original, or non-standard component of the core methods in this research? Note that if the LLM is used only for writing, editing, or formatting purposes and does not impact the core methodology, scientific rigorosity, or originality of the research, declaration is not required.

Answer: [NA]

Justification: LLM is used only for writing, editing, or formatting purposes.

Guidelines:

- The answer NA means that the core method development in this research does not involve LLMs as any important, original, or non-standard components.
- Please refer to our LLM policy (<https://neurips.cc/Conferences/2025/LLM>) for what should or should not be described.